	nBLM – PDR1.2	CEA-ESS-DIA-RP-0027
	ESS-I	Page 1 over 61

NBLM SYSTEM

PDR 1.2

S. Aune, Q. Bertrand, D. Desforge, F. Gougnaud,
Tom Joannem, P. Legou, J. Marroncle, Y. Mariette,
V. Nadot, T.Papaevangelou, L. Segui, G.Tsiledakis






	nBLM – PDR1.2	CEA-ESS-DIA-RP-0027
	ESS-I	Page 2 over 61

TABLE OF CONTENTS

1. Introduction	5
2. Prototypes and initial tests	6
2.1. Mechanics	6
2.2. Micromegas detector	9
2.3. First full prototype montage	12
2.4. Detector tests with pre-prototype and signal characteristics.....	12
2.5. Cable length – effect on the signal rise time	15
3. On-Board Front End Electronics initial design.....	18
4. Gas system	20
4.1. Gas system overview and general characteristics.....	20
4.2. Design and P&ID Diagrams.....	21
4.2.1. Bottle storage area	21
4.2.2. Gas Distribution System	24
4.2.3. Gas line system for group of detectors.....	27
4.2.4. Gas Rack and PLC controller	29
4.3. List of components.....	30
5. Control System.....	31
5.1. Requirements for the control	31
5.2. Architecture overview	31
5.3. Detector controls	32
5.3.1. CAEN High Voltages control.....	32
5.3.2. Low voltages control	32
5.4. Fast acquisition	33
5.5. FPGA software	33
5.6. System architecture at Saclay.....	33
5.7. Gas control	34
5.7.1. Gas control architecture.....	34
5.7.2. Gas control presentation.....	35
6. nBLM distributed architecture.....	36
6.1. Detector position and racks	36
6.2. Cables specifications and number.....	39
7. Response to ESS scenarios.....	40
7.1. Response for 1% 1 W/m losses compared with accidents	40
7.2. Conclusions for the 1W/m case and the accidental one rates.....	51
7.3. Threshold between “thermal” and fast neutrons	53
7.4. Detector position results by simulations	53
7.5. Using borated rubber instead of Cd	56
8. Recompile of points to discuss.....	57



 	nBLM – PDR1.2	CEA-ESS-DIA-RP-0027
	ESS-I	Page 3 over 61

9. Answers to questions from PDR1.1 review	58
10. Bibliographie	60
Appendix 1.....	61

 	nBLM – PDR1.2	CEA-ESS-DIA-RP-0027
	ESS-I	Page 4 over 61

Acronyms

Name or acronym	Definition
BEE	Back-End Electronics
BIS	Beam Interlock System
BNC	Bayonet Neill–Concelman (Connector)
CA	Channel Access
CEA	Commissariat à l'Energie Atomique
CPU	Central Processor Unit
DTL	Drift Tube Linac
EEE	ESS EPICS Environment
ESS	European Spallation Source ERIC
EPICS	Experimental Physics and Industrial Control System
ESSI	ESS Irfu project
FEE	Front-End Electronics
FPGA	Field Programmable Gate Array
GND	Ground
GUI	Graphical User Interface
HEBT	High Energy Beam Transport
HWR	Half Wave Resonator
IKA	In-kind agreement
I/O	Input / Output
ICS	Integrated Control System
LCS	Local Control System
LINAC	Linear Accelerator
MEBT	Medium Energy Beam Transport
MPGD	Multi Pattern Gaseous Detectors
MPS	Machine Protection System
MTCA	Micro Telecommunications Computing Architecture
nBLM	Neutron sensitive Beam Lost Monitor
PCB	Printed Circuit Board
PDR	Preliminary Design Review
PLC	Programmable Logic Controller
PV	Process Variable
P&ID	Piping and Instrumentation Diagram
SAR	System Acceptance Review
SMA	SubMiniature version A (Connector)
SoW	Scope of Work
SHV	Safe High Voltage (Connector)
TBC	To Be Confirmed
ToT	Time Over Threshold

 	nBLM – PDR1.2	CEA-ESS-DIA-RP-0027
	ESS-I	Page 5 over 61


1. Introduction

This report presents the status of the nBLM system, focusing on the first design of the electronics (milestone #5 of IKA Schedule_AIK 7.9). Different aspects of the project are also discussed as the gas system design, the architecture of the acquisition and control system and the expected response of the detectors under ESS scenarios obtained through MonteCarlo simulations. In addition, the characteristics of the signal and the analysis strategy to identify neutrons are also presented.

Complementing this PDR1.2, different documents are also delivered:

- The P&IDs of the gas system
- The results of the MonteCarlo simulations is detailed in document [1]
- The list of suggested material for the gas system control

ERRATUM for PDR1.1: the results shown in the PDR1.1 corresponding to the studies of the response to ESS scenarios of the slow and fast module were done with He+10%CO₂ and no with pure He as indicated in the text. The gas that we plan to use at ESS is He+10%CO₂.

	nBLM – PDR1.2	CEA-ESS-DIA-RP-0027
	ESS-I	Page 6 over 61

2. Prototypes and initial tests

The first two prototypes of each detector, slow and fast, have been ordered in January 2017. The mechanical design was included in PDR1.1. The 3D view of the assembly of both detectors is shown in Figure 1 and the plan of each one separately is presented in next section. The mechanical parts of both first prototypes have arrived to Saclay in April and May 2017. Some pictures are shown also in next section.

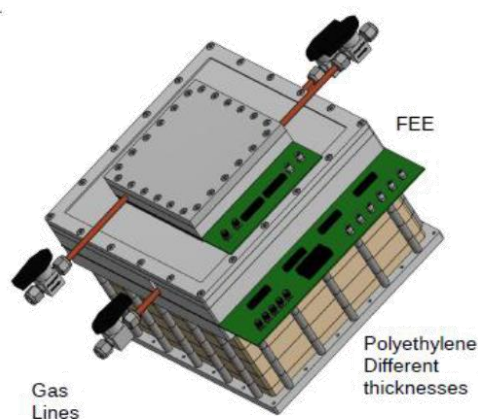


Figure 1: 3D drawing of the nBLM prototype. The “fast” module is seen in the front-top side of the detector, while the “slow” module is attached behind it, surrounded by the polyethylene.

2.1. Mechanics

The details of each design were included in PDR1.1. As a reminder, here we include the last 2D drawings in Figure 2 and Figure 3 for the slow and fast module, respectively. Pictures of both detectors are shown in Figure 4.

The characteristics of the Micromegas detector are explained in more detail in section 2.2. In both detectors (slow and fast) it will consist on an active area of $7 \times 7 \text{ cm}^2$ (item 1 in Figure 2). The main modification with respect the PDR1.1 is the reduction of the PCB area on the sides of the detector to reduce PCB area waste. In addition, for the slow detector prototypes, we have decided to mount just a single-face Micromegas instead of two placed back-to-back. However, the same chamber can be operated with a double-face Micromegas, without any modification. For the final design, the selection between single or double detector will be done accordingly to the needed efficiency (the double detector is twice efficient than the single one).

The first $^{10}\text{B}_4\text{C}$ deposition was done at Saclay with a thickness of $0.8 \text{ }\mu\text{m}$. This is installed in the entrance of the drift region of the slow detector. In the case of the fast detector the detection of the neutrons is done through the neutron-proton recoil in a plastic foil. Therefore, a polyethylene or polypropylene layer is used in order to create them. A 2-mm layer has been metallized in Saclay with

an approximate thickness of 50 nm Al. As a second option we have used a stretched aluminized Mylar of 50 μm , glued on an aluminium plate.

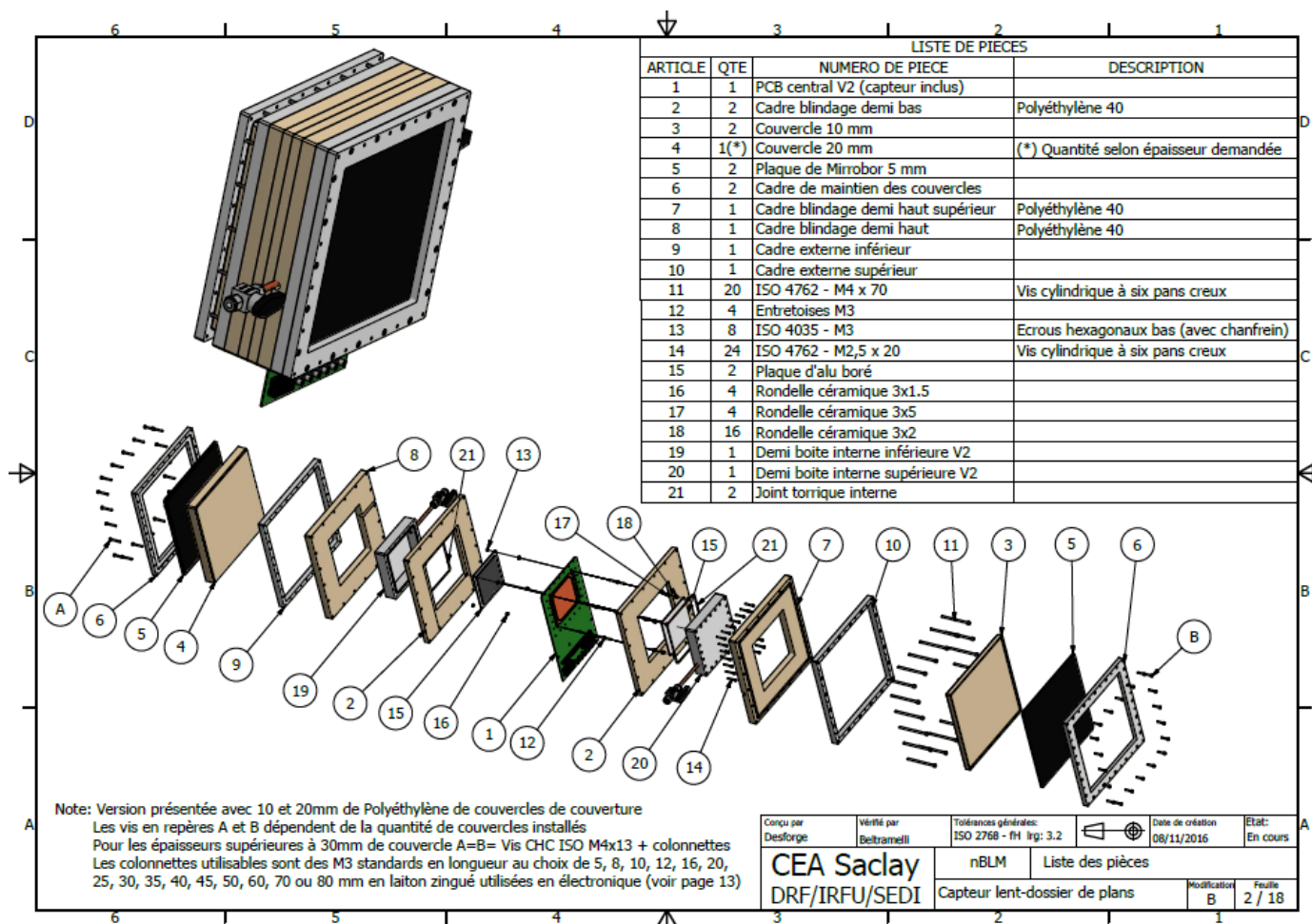


Figure 2: View of the mechanics of the slow module

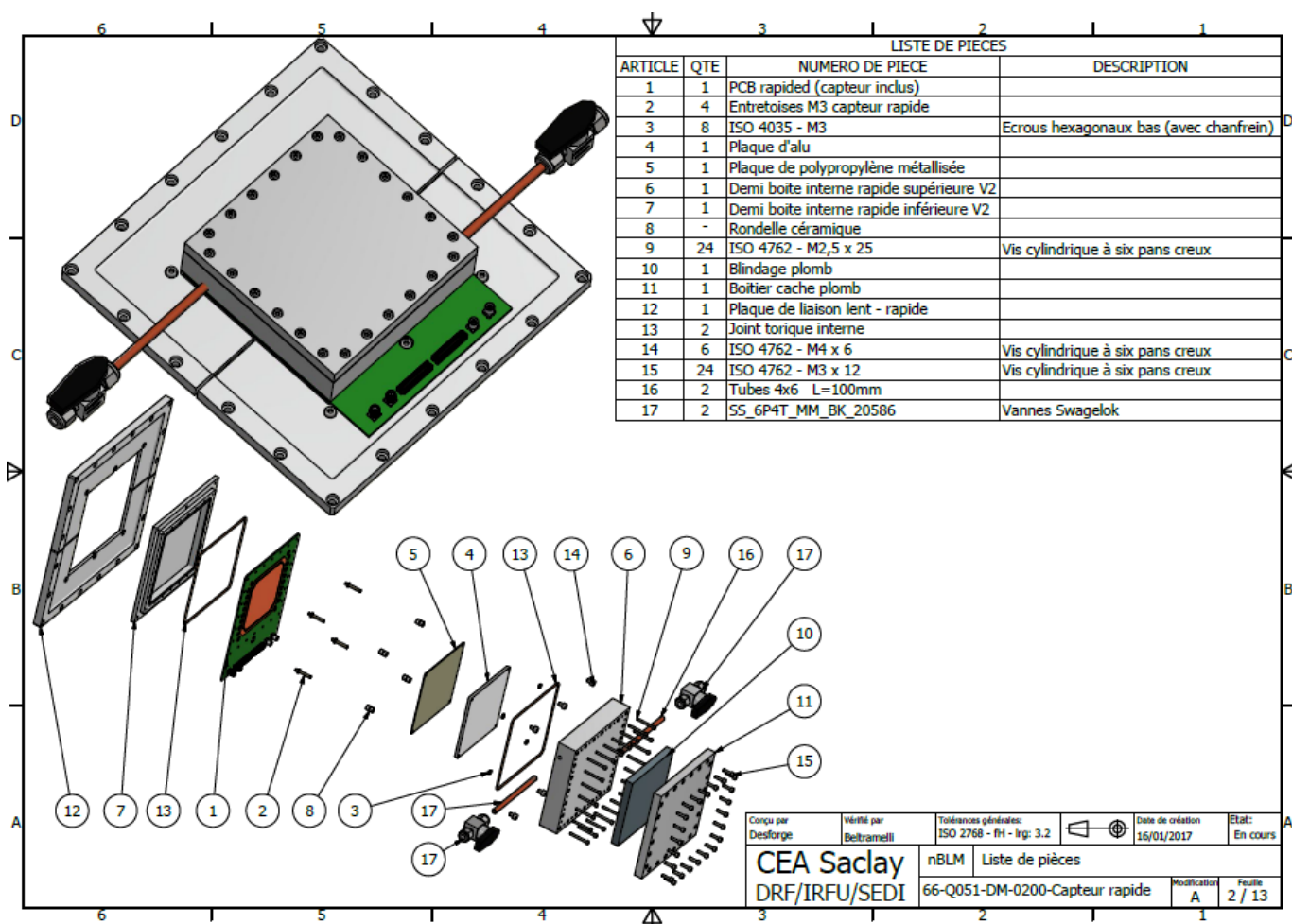


Figure 3: View of the mechanics of the fast module.

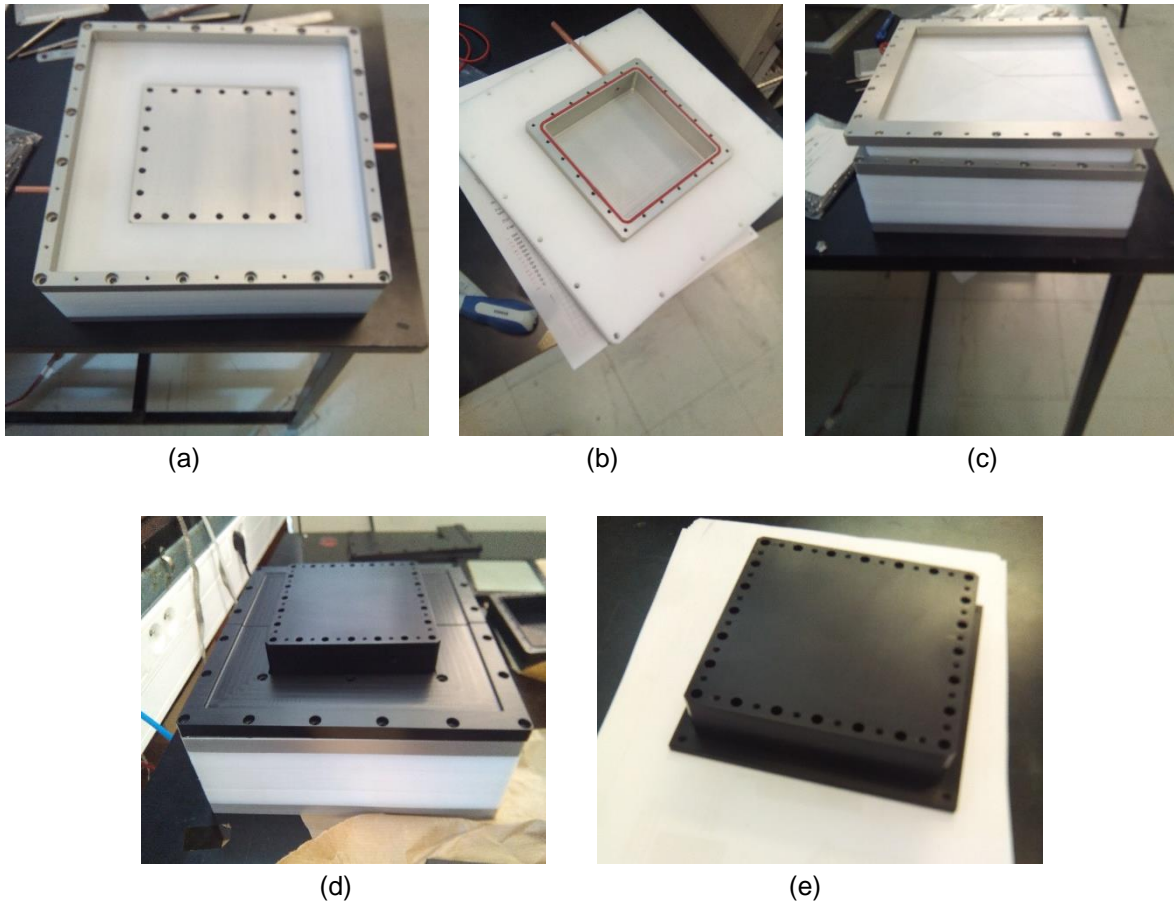


Figure 4: Pictures of the mechanical parts of the prototypes. (a)-(c) Slow module, in (b) with the chamber open. In (c) showing the possibility to add more polyethylene thickness. (d) and (e) correspond to the fast module. In (d) attached to the slow module. However, both can be separated and tested alone. As we can see, in (e) we have the fast module separated from the slow. Both gas chambers are identical in dimensions.

2.2. Micromegas detector

The detector readout scheme is the same for both fast and slow prototypes and will be based on bulk Micromegas technology [2]. It consists in a 4-layers PCB, strips, spacers and the micromesh attached on the PCB using the bulking process. A drawing of the mechanical design can be seen in Figure 5. The active area is $\sim 7 \times 7 \text{ cm}^2$. The FEE will be placed on board, connected in the space left at the front of the board. 6 detectors (3 for the slow and 3 for the fast) have been ordered to CERN and were expected in May 2017. However, they were delivered only on the 20th of June, due to some unexpected delays on the MPGD workshop. We can see a picture of one of them already mounted with the electronics in Figure 6 bottom. The rest of the prototypes and the production of the 42 modules will be done at Saclay in the bulk laboratory lead by Stephan Aune.

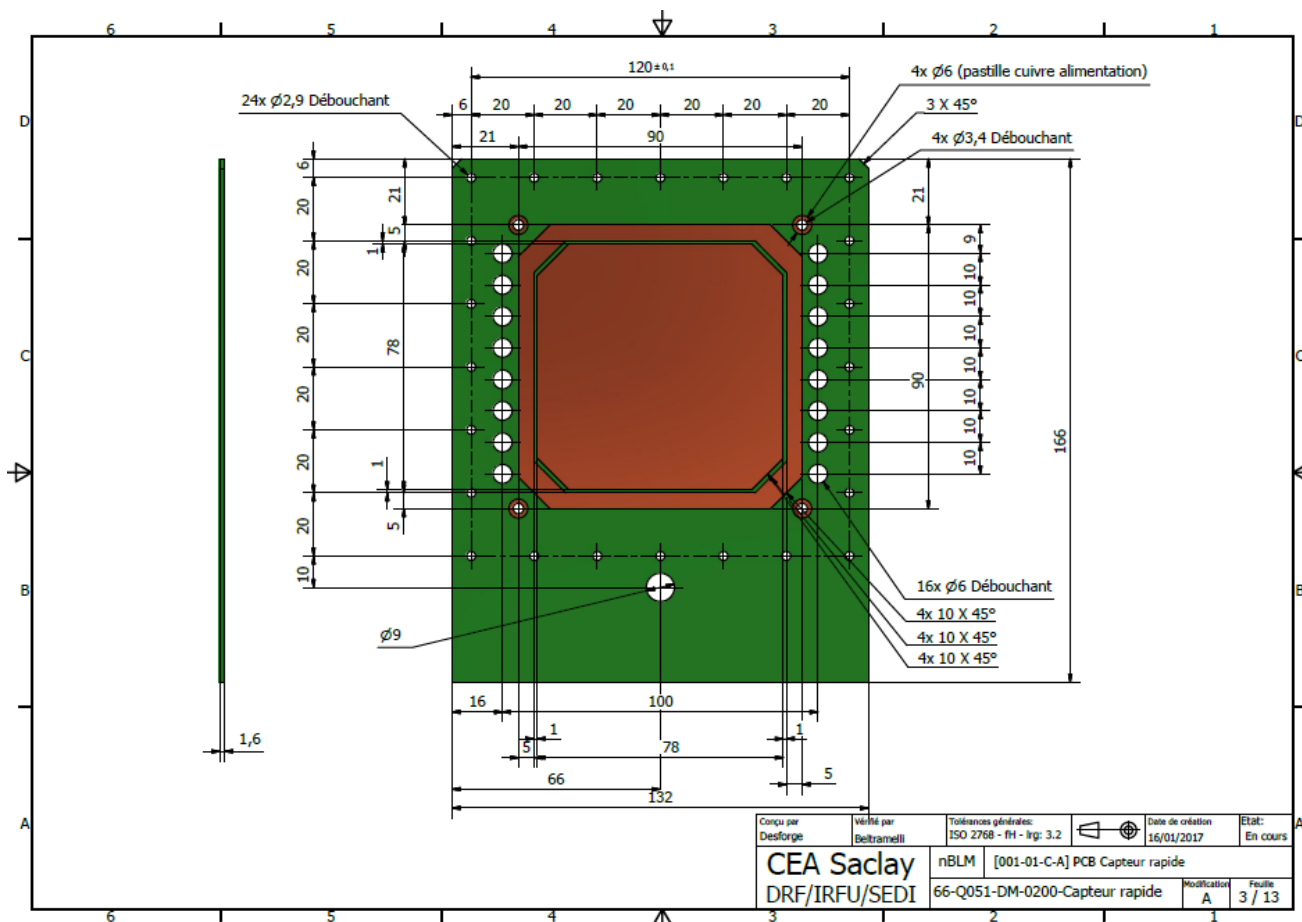


Figure 5: Design of the PCB board from the point of view of the mechanics.

The routing of the PCB was done between Philippe Legou and the CERN MPGD workshop. In Figure 6 we can see the PCB electronics design. The active area is segmented in 4 strips, each one read independently and with a preamplifier on board for each line. The output signals are read via SMA connectors. Also, on the top left part we can see the connection for the low voltage ($\pm 5V$ and ground for the amplifiers). A filter will be also included to protect the amplifiers from possible discharges in the detector during the commissioning. On the bottom left part of Figure 6 there will be the connectors for the high voltage for the mesh and the cathode (drift region). These voltages will be of the order of 2 kV maximum for the cathode and few hundreds of volts for the mesh.

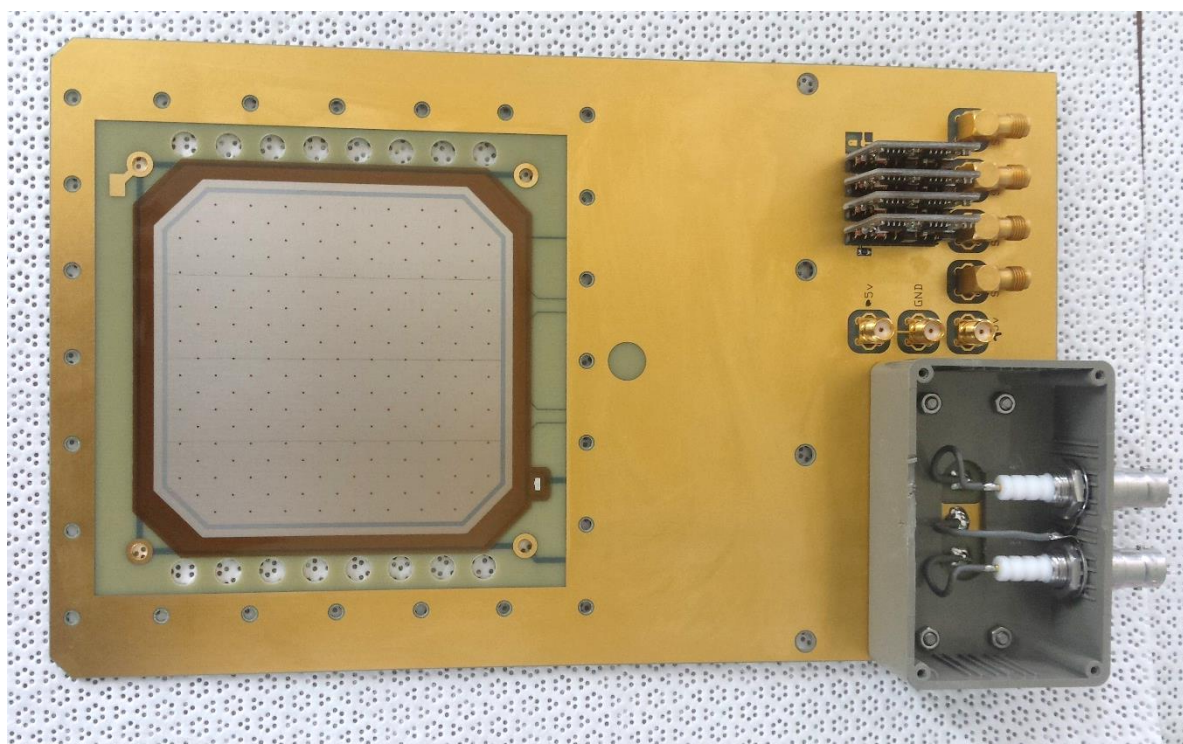
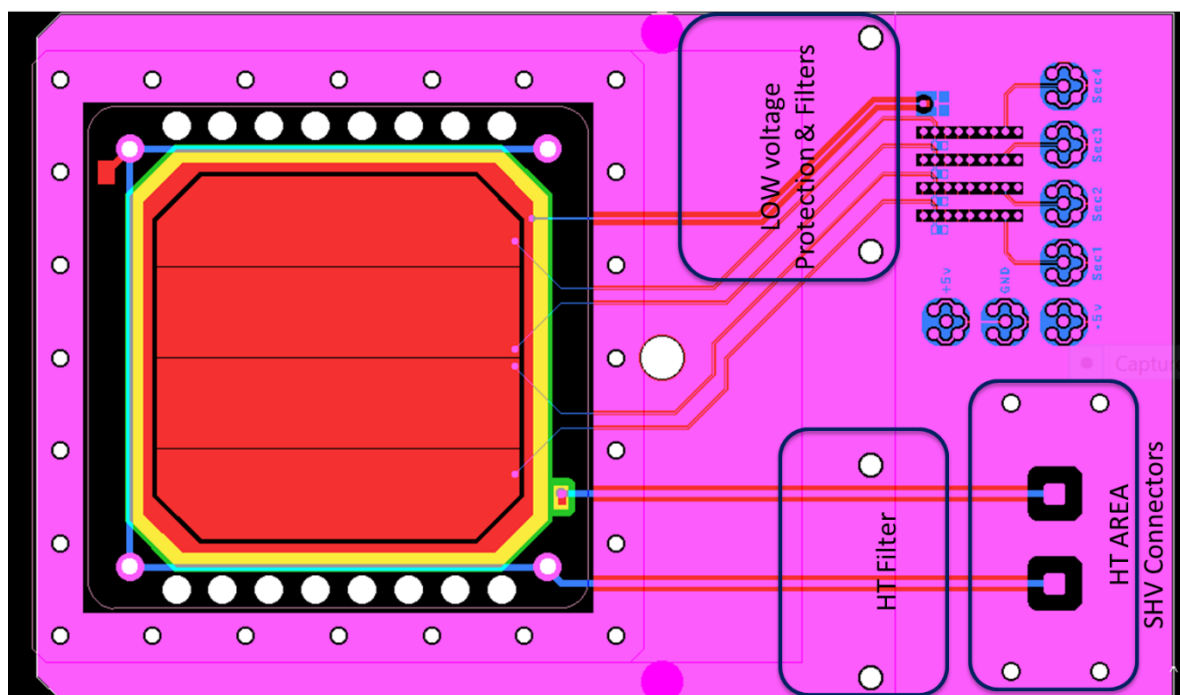



Figure 6: (Top) Design of the Micromegas PCB. The active area of the detector, or anode, will be segmented in 4 strips. Each line can be read independently. Each via goes to a preamplifier and is read via an SMA connector. The high voltage to the mesh and drift is fed by SHV connectors. For both the high and low voltage we have a filter and for the low voltage also a protection to protect the PA from possible discharges. The preamplifiers low tension is also included in the board. (Bottom) First Micromegas received, mounted with the different electronic components.

	nBLM – PDR1.2	CEA-ESS-DIA-RP-0027
	ESS-I	Page 12 over 61

The preamplifier needs a power of $\pm 5V$. Its quiescent current is 10mA, which means a consumption of 100 mW for each preamplifier. The noise is $\sim 600\mu V$ rms and the input signal can be positive or negative. The rise time is $< 1ns$. Its gain can be modified during the design to accommodate to the specific requirements of each detector (the gain can be tuned to be different for each detector placed at different locations, depending also on their use either for monitoring either for safety).

2.3. First full prototype montage

The first slow detector has been mounted the 22nd of June 2017. In Figure 7 left we can see the different parts needed and the detector once closed (right). The detector has been placed in gas on the 28/06/2017 and will be tested in the following days.

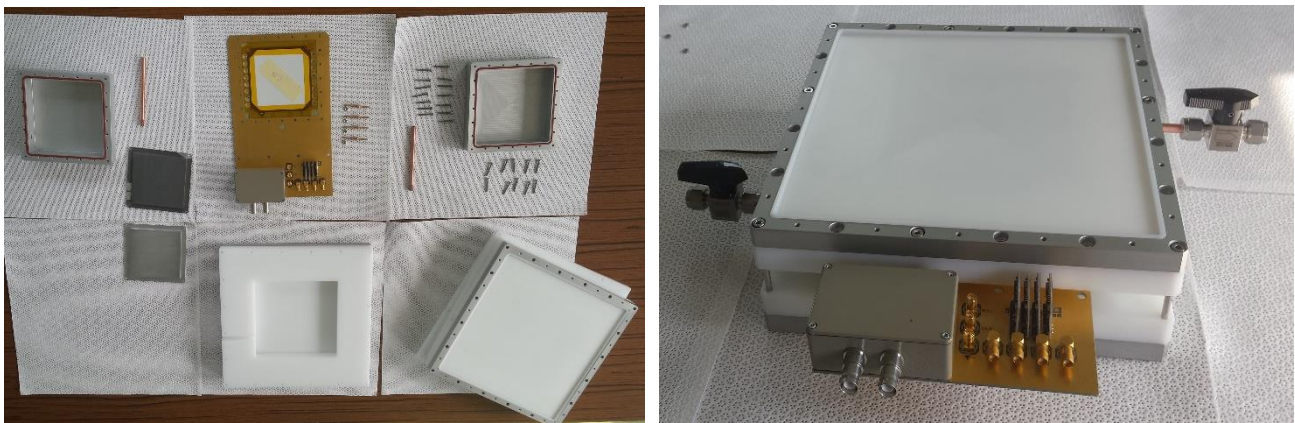



Figure 7: (Left) The needed elements to install a slow module. We can see the gas chamber with the O-ring in place. The Micromegas with the FEE on board. One aluminium plate without and one with the $^{10}B_4C$ converter (black piece) and the polyethylene pieces. (Right) The detector closed and with the gas input and output lines. In this case has been mounted with a moderator thickness of 20 mm.

2.4. Detector tests with pre-prototype and signal characteristics

Due to the unexpected delay in the fabrication of the Micromegas prototypes (expected by mid-April and arriving finally the 22nd of June), we have performed some tests with a similar detector, which was made available by Georgios Tsiledakis (who also contributed to this data taking).

The detector consists on a metallic chamber with a gas entry and exit to recirculate the gas, very similar to the one we will use in the prototypes. The detector has been surrounded by a shielding of polyethylene with borated rubber outside and the ^{252}Cf in the middle, just below the shielding + chamber. The gas used was He+10%CO₂. The Micromegas used is a bulk with a gap of 128 μm . The drift distance is 1mm. In the entrance of the drift distance there is a $^{10}B_4C$ deposited in an aluminium plate of 1.5 μm .

	nBLM – PDR1.2	CEA-ESS-DIA-RP-0027
	ESS-I	Page 13 over 61

Different elements have been tested with this setup:

- Preamplifiers
 - Current amplifiers, designed by Philippe Legou → good S/B ratio, good gain, spark protection. After the tests they are the preferred option for the final detectors.
 - Cividec C2 2GHz – 40db (high cost fast preamplifier, to be used as reference).
 - CAEN charge amplifier model 1425 (for comparison with the current amplifiers).
- Long cables
 - 50 m low loss cables (Y-195)
- Acquisition card
 - ADC-3111 with VME board (IFC1211)
 - MTCA-CAENELS
 - In both cases we can see the signals clearly in the GUI (see Figure 8)

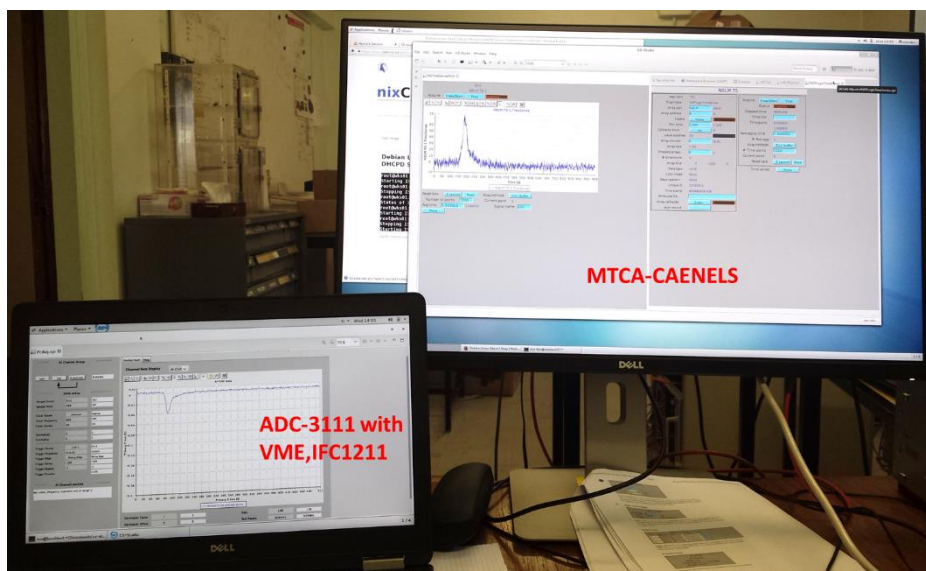



Figure 8: Neutron event detected in pre-prototype from a Cf source with two acquisition cards. We can see a good S/B level.

In addition, the tests have served to start developing the pulse analysis to help in the FPGA algorithm definition and in the needed requirements and functions for the EPICs communication. This is discussed in an independent document in more detail [3], although it is a first version still in evolution. In the following, we show the signal characteristics and the analysis strategy. In Figure 9 it is shown a real neutron event detected in the setup explained before. We were using a ^{252}Cf source. It emits neutrons with a mean energy of $\sim 1.5\text{MeV}$. The neutrons are detected via a $(n,\alpha)^{10}\text{B}$ reaction. The emitted alpha will ionize the gas and produce an electric signal in the Micromegas. Each alpha detected produces a pulse which amplitude is proportional to its energy.

	nBLM – PDR1.2	CEA-ESS-DIA-RP-0027
	ESS-I	Page 14 over 61

Each electric pulse is sent to the ADC card. A trigger level will decide if the event is recollected or not. Once in the ADC the FPGA algorithm will do the analysis to determine if the signal was produced by a neutron or not. Some relevant parameters to define for pulse shape analysis that will be implemented in the FPGA programming are:

- **Pedestal:** The offset level. It is measured with the beam off for each detector and stored. Then it is subtracted from each pulse before proceeding to the calculations of the different variables.
- **Trigger:** Level above the pedestal (value to be tuned according to the results of the plan). It can serve to discriminate between gammas and neutrons.
- **Maximum amplitude**
- **Rise Time:** defined in general as the time between the 10% of the maximum amplitude and the 90% of the maximum amplitude
- **Charge:** defined as the integral of the pulse. It can also serve for gamma-to-neutron discrimination, especially if it is combined with the maximum amplitude.
- **Pulse duration:** Time between the bins that are defined as start and end of the pulse. Typically it is where the pulse rises over and falls under the signal noise level or the 10% level. The pulse integration for the charge calculation is done between those limits.

Other variables useful to discriminate between “good” and “bad” pulses could be:

- **Charge over amplitude (Q/A):** ratio between the charge and maximum amplitude for each pulse. For the correct ones should be a constant as we always have a constant energy. For a noisy event or a spark will be different.
- **Time Over Threshold (ToT):** is similar to the pulse duration but not exactly the same. It is the duration of all bins above the trigger level. We count events with a ToT above a given value.
- **Current:** Continuous integration in different determined time windows.

Once these variables are calculated for each pulse they are compared with a range of values stored externally that defines a neutron. In the final analysis it is probably that only some of these parameters will be needed. More studies are on-going to choose the correct ones. In this section the procedure we will follow is shown. If accepted as a neutrons, the event is added to the neutron counter of the corresponding detector. A rate for different time windows will be obtained. The number of neutrons per μs could serve for the safety of the accelerator. It can be sent to the BIS for MPS for further analysis or it can be directly compared with a reference rate value for optimal operation and if it is above it sent an alarm directly to the MPS. The values of the variables will depend on the gain of the detectors. They need to be determined experimentally for each one.

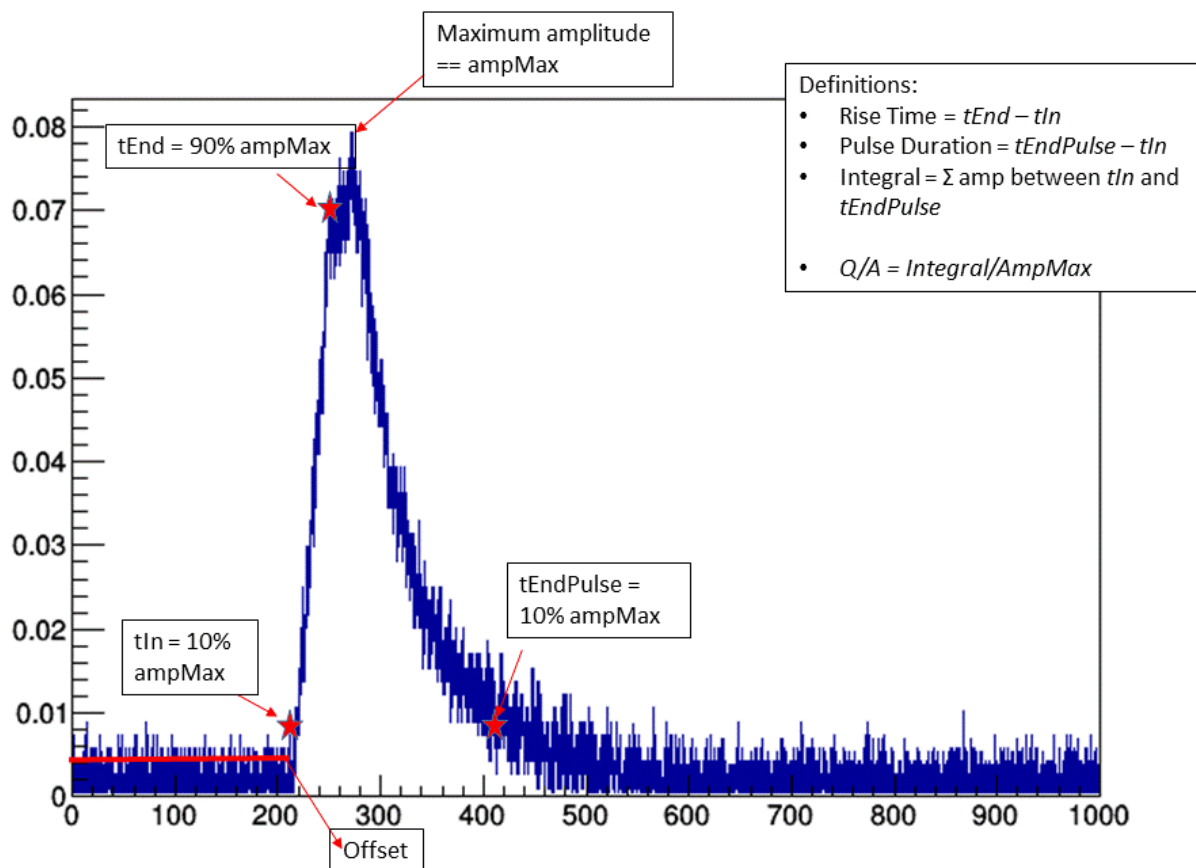


Figure 9: Typical signal from Micromegas produced by a $^{10}\text{B}_4\text{C}(n, \alpha)$. It is clearly identified over the noise and the variables to be computed are also indicated: rise time, amplitude, duration and integral of pulse.

2.5. Cable length – effect on the signal rise time

Once installed at ESS, the mean signal cable length will be about 50 m. In the best case this distance could be reduced to ~20 m, and in the worst case can be > 100 m. Several tests have been performed to study the effect of the cable length in the signal propagation. In general, in typical coaxial cable there is a delay of ~5ns/m.

The typical signal in a Micromegas detector (explained in detail in previous section) has a rise time of ~40-50 ns, with a duration of ~100-200 ns due to the ion tail. Tuning the operation settings of the detector we can differentiate between the electron peak (few ns duration) and the ion tail. However, after more than 50 m of cable we will lose this separation (Figure 10). Also, in order to operate in this regime we need preamplification, i.e. very high tension in the drift region, which can cause instabilities in a long term operation (not advisable for a safety system).

The effect of the cable length in the rise time has been measured experimentally at Saclay by Philippe Legou using a pulser (Lecroy 9210) to inject pulses of different rise times (accuracy of 1 ns) into different cable lengths and using an oscilloscope to read them at the other side of the cable (Oscilloscope Tektronix DPO 4104B). In Table 1 and in Figure 11 we show the experimental results: 20 meters length starts to include an increase in the rise time with respect to the initial rise time of the signal. The effect is stronger for shorter initial rise times. For example, with a cable of 40m, for an initial signal of 5 ns rise time, the output signal has a rise time of ~ 17 ns, while for an initial signal of 35 ns rise time, the output after 40 m is ~ 40 ns.

In addition, we can compare the signals using a 50 m or a shorter one (~ 1 m) when operating in no preamplification. The long cable is a low loss coaxial cable (Y-195). We compare the pulse from the scope in Figure 12. We can see how the cable introduces a delay of about 150 ns. The rest of the characteristics seems not to change much.

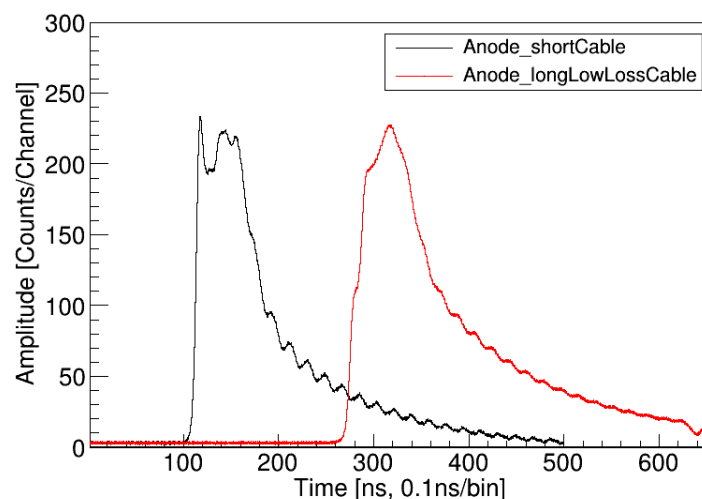


Figure 10: Pulse obtained in preamplification mode with a short (black) and long cable (50m, red). The separation between electron and ion tail disappear when using the longer cable.

Cable Length (m)	Rise time (ns)
5	1.125
10	1.334
15	2.314
20	3.895
25	6.573
30	9.691
35	12.727
40	15.162

Table 1: Rise time after a cable of different lengths (input signal 1ns rise time).

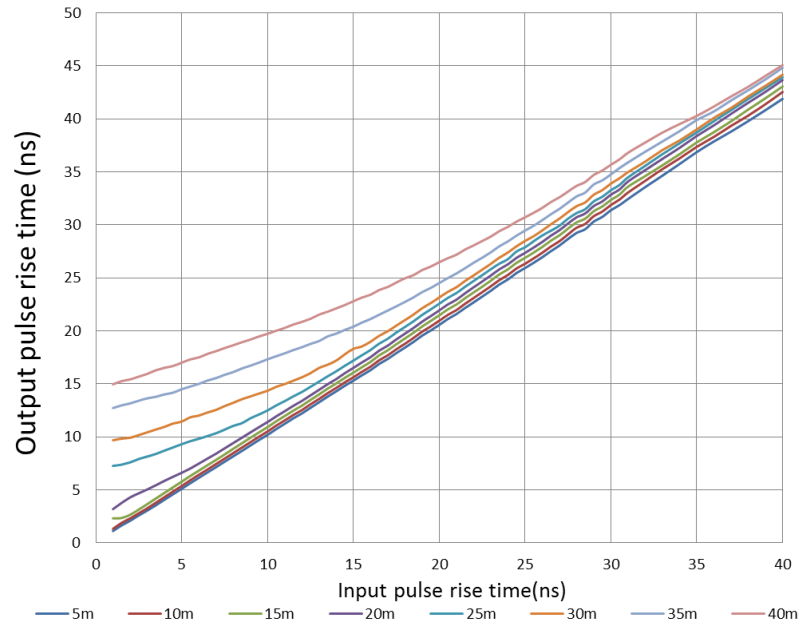


Figure 11: Effect of cable length on the signal rise time after propagation

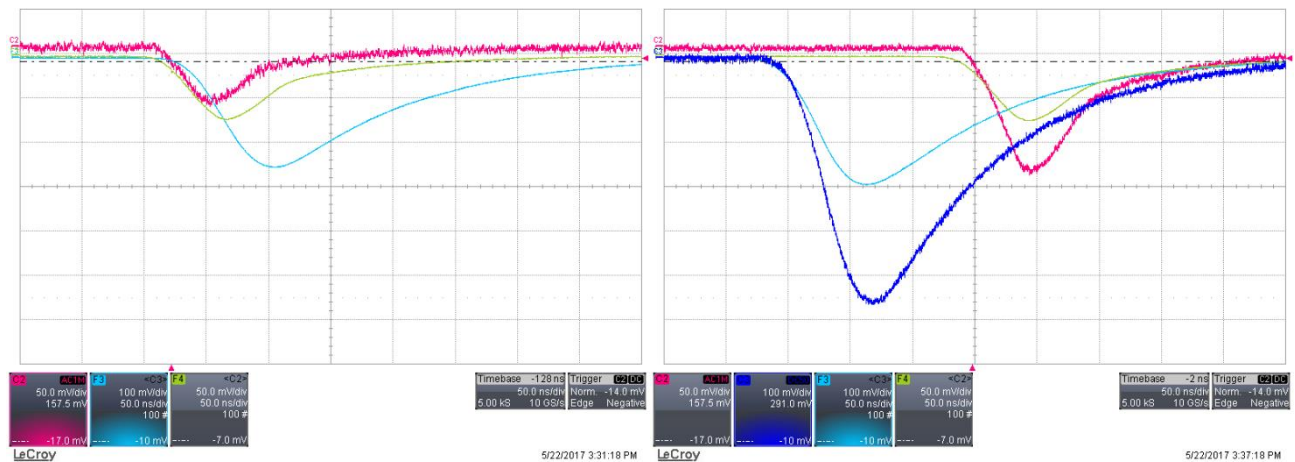



Figure 12: Screenshot from scope of two neutrons events. We measured simultaneously the mesh (blue with a CAEN charge preamplifier) and the anode (red measured with the Cividex preamplifier). Also an average over 100 pulses is shown (cyan for the mesh, green for the anode). The left side the anode is read with the short cable and in the right side with a long cable of 50m. We can see how the 50 m cable introduces a delay of about 150ns.

	nBLM – PDR1.2	CEA-ESS-DIA-RP-0027
	ESS-I	Page 18 over 61

3. On-Board Front End Electronics initial design

The FEE will be integrated on the PCB themselves. With the amplifier on board we limit the signal loss during the transport of the electrical pulse as it is amplified before sending to the BEE, through the ~50m cable. This implies that the amplifiers should be radiation resistant for the long-term operation in the ESS conditions. We are considering two possibilities for the integration on the board:

1. Design a mezzanine plug-n-play card with the preamplifiers and connectors on it which is connected on the board. The advantages are, for example, in case some component of the electronics fail, we only need to change this mezzanine card, we don't need to remove the detector, open it and change the PCB. In addition, for the tuning of the system during commissioning, we can have several cards prepared with different gains to choose the optimal one in each case. This could also simplify the development of cost-efficient radiation hard preamplifiers.
2. Elements directly on-board. Better for noise and more compact, however an intervention implies the dismounting of the chamber.

We consider option 1 more convenient.

The design concept for the FEE for the prototypes to be used for the tests is shown in Figure 13. The detector will have 4 strips, as in the case of the pilot prototype. Each output strip will be connected to a preamplifier. They will have the same characteristics as the ones explained for the prototypes. However, in the baseline of the project only one output per detector is foreseen. Therefore, with the help of jumpers, we can select to read from 1 up to the 4 strips together, using a sum integrator. The decision about reading 1, 2, 3 or 4 strips will take place during the commissioning or the tests of the detectors. In addition, this option allows to disconnect one of the strips if it presents a bad functioning after operation during some time and in the case the replacement of the full detector is not needed. The consumption for the preamplifiers, splitters and sum integrator is 600 mW. The sum integrator introduces a delay of only ~2ns. An output driver buffer will be placed before the SMA output to improve the transmission of the signal over the cable length. The quiescent current for one buffer is 15mA, so for one buffer the consumption is 120mW. The polarization voltage for the preamplifiers is +5V and -5.2V.

Depending on the dimensions of the final detector, we can:

1. Have one preamplifier for each channel (appropriate for large areas)
2. Or we can have the sum from 1 to 4 strips and one amplifier after into one single readout if the area (capacitance) is small enough.

The option 1 has a higher power consumption as the 4 independent preamplifiers will be in continuous operation, despite which channels we finally use for the analysis. However, the second one can only be implemented in small area detectors due to the higher capacitance (noise) in larger ones.

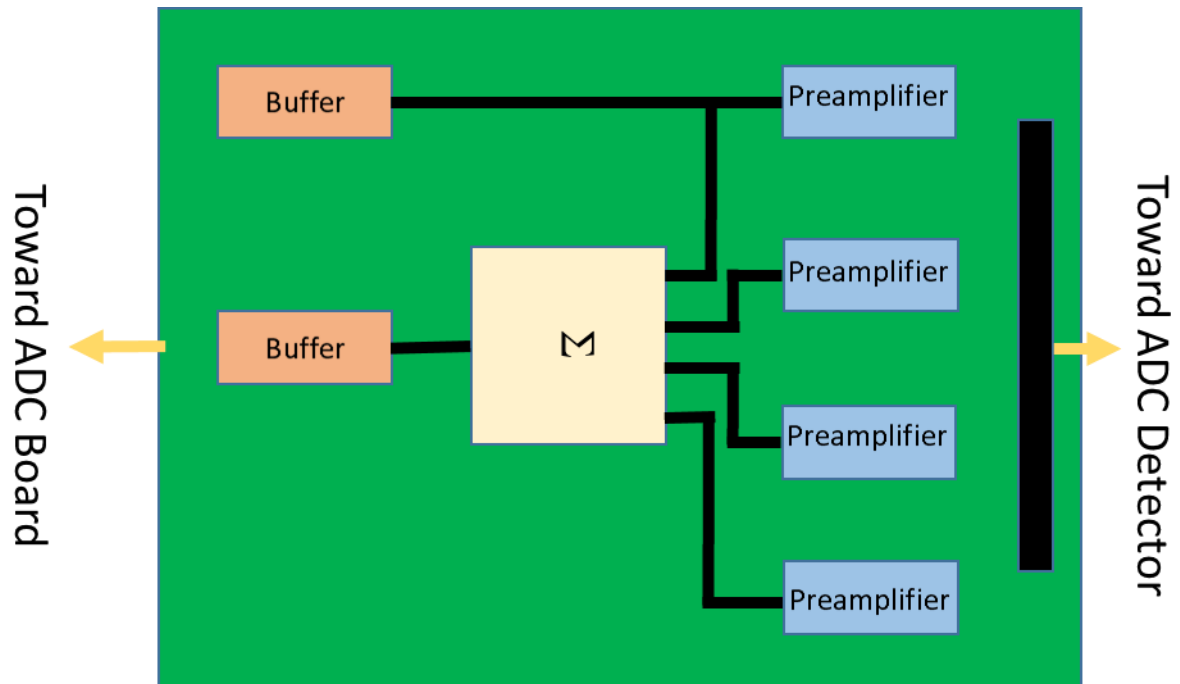



Figure 13: Schematic view of the FEE layout. Each strip of the detector will be connected to a preamplifier. We will then have the option to read 1, 2, 3 or 4 of the signals together, either using a jumper on-board or changing the mezzanine card. In addition, a buffer will be placed after the sum of the signals to improve the signal transmittance to the BEE through the long cables.

Connectors

- SHV for the high voltage of mesh and cathode
- SMA for low voltage and signal

	nBLM – PDR1.2	CEA-ESS-DIA-RP-0027
	ESS-I	Page 20 over 61

4. Gas system



Micromegas detectors are gaseous detectors, therefore, the nBLM system will need the use of gas to operate. The system will work in recirculation mode with an exhaust line, and with a constant flow in all the detectors. Gas lines will be driven from the outside of the building, where the gas bottles will be stored, into the service tunnel where we will have the distribution rack, and from there to the tunnel to feed the detectors.

In this section, the general characteristics of the system are discussed, showing the P&IDs of the different parts (they are also send externally in the distribution of this document). The control of the system is done through PLC that can communicate with EPICS and is discussed in section 5.7.

4.1. Gas system overview and general characteristics

The main requirement of the system is to present a high reliability while keeping the operability of the 42 modules stable. We start from the premise of a simple concept but redundant and with control command with PLC, to, for example, monitor the leaks (flow monitoring). The specifications of the gas type and flow are:

Gas type	He + 10% CO ₂	Used of premixed bottles
Total flow	8 - 16 l/h (feeding/exhaust lines)	Limitation of possible maximum flow immediately after gas bottle at ~20-30 l/h with a rotameter (0-50 l/h)
Flow per line	1-2 l/h (distribution/return lines)	Detectors in series
Pressure after bottle	2 bar total	Release valve at ~7 bar
Pressure for distribution	1atm + 200 mbar (tbc)	Depends on final pipe cable length
Pressure at exhaust	1atm + 50 mbar	Pressure and flow will be controlled by PLC. Safety release valve immediately after gas bottle to assure no more pressure in the line and system than the limit.

 	nBLM – PDR1.2	CEA-ESS-DIA-RP-0027
	ESS-I	Page 21 over 61

The specifications of the pipes are:

- Preference stainless steel
 - If copper, use clean copper
 - Can be flexible stainless steel hose in stubs (if finally goes through stub) and rigid before/after
 - Connection to detector could be made by polyethylene tubes to avoid parasitic electrical noise to be picked-up by the signal cable. It could be just after the shut-off connector shown in Figure 19, maximum 1m length per detector.
- Connection on metric system
- Dimensions:
 - 6/8 mm (inner/outer) for the IN/OUT lines and the distribution/return lines
 - 4/6 mm (inner/outer) for the connection to each detector.

4.2. Design and P&ID Diagrams


The second version of the P&IDs have been prepared after discussing the first version prepared in January 2017. The gas system consists in 4 parts:

- The bottle storage area outside the building
- The gas rack where we have the control command
- The distribution and return lines from (to) the rack to (from) the accelerator tunnel
- The detectors localization where the lines will connect to each module

We propose to install 2 IN / 2 OUT lines from the bottle storage area to the rack (one will be in used, the other being spare). From the rack 5+3 spare distribution lines and 5+3 return lines will be passed to the accelerator tunnel. They will be connected in parallel and each one will feed a group of detectors connected between them in series. All the instrumentation controlled by software will be installed in the service tunnel, i.e. will be also accessible during running. We will be able to close the valves of one group of detectors while running the others.

4.2.1. Bottle storage area

We suggest to have a bottle storage area with 2 stacks of 6 bottles of premix He+10%CO₂ outside the accelerator (at open air) protected by a shelter as discussed with Marcus Green and shown in Figure 14. Six B-50 bottles (50 liters) of 200 bar each assure the gas of the system for 250 days. As it can be seen in Figure 15, from the bottles we will control the pressure of the stacks (to know when to exchange between them), adjust the pressure to 2 bar, have a purging valve (for when

	nBLM – PDR1.2	CEA-ESS-DIA-RP-0027
	ESS-I	Page 22 over 61

we exchange the stacks), then a rotameter to adjust the maximum flow to ~30 l/h and a release valve at ~7 bar.

The bottles specifications are:

- Premix He + 10% CO₂
- 200 bar bottles → 50 l
- Operating at 1 bar, 6 bottles last 250 days
- Purity for each gas 5.0 (99.9990 %)



Figure 14: Possible 2x6 gas storage shelter

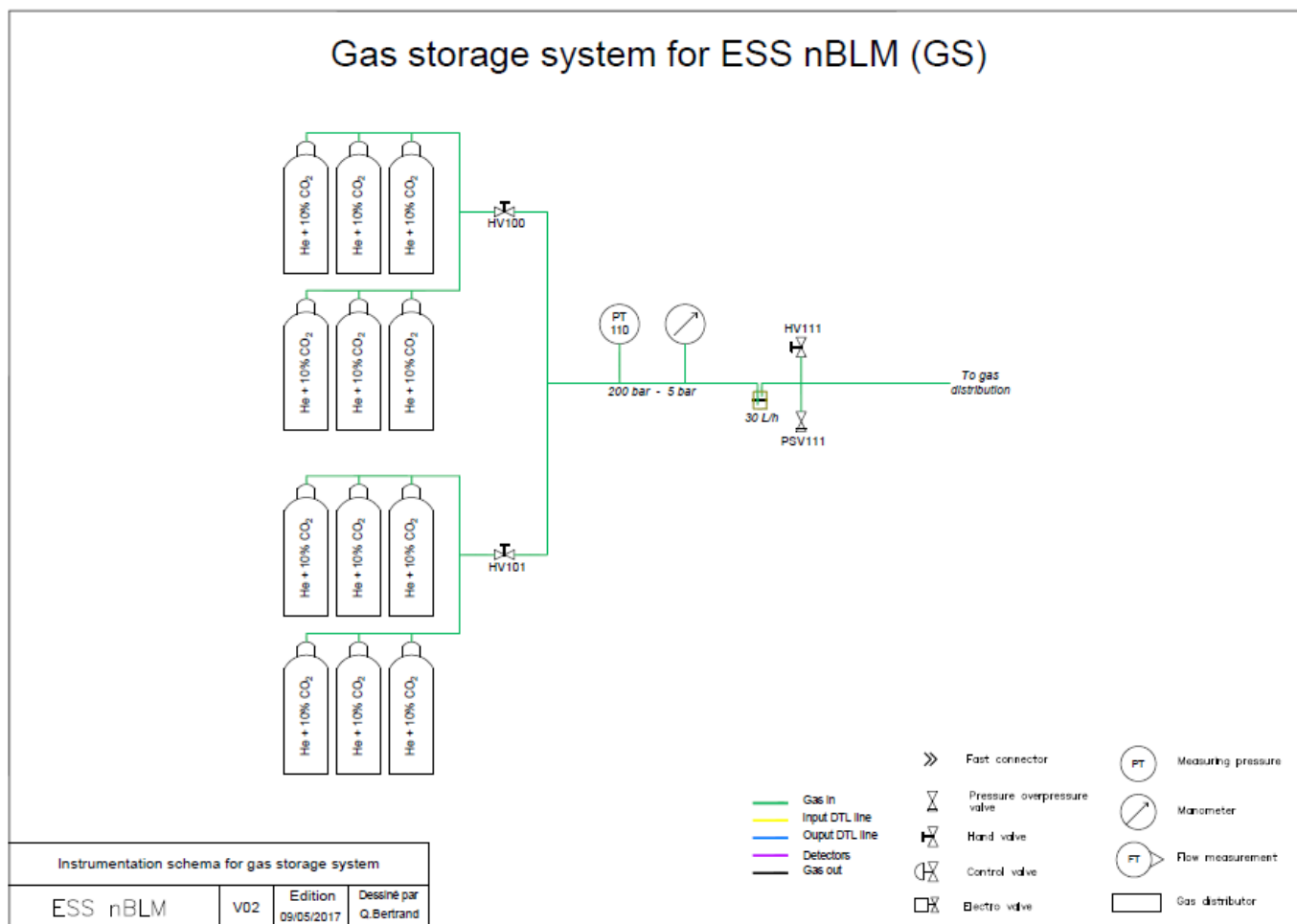



Figure 15: P&ID of the bottle storage area.

	nBLM – PDR1.2	CEA-ESS-DIA-RP-0027
	ESS-I	Page 24 over 61

4.2.2. Gas Distribution System

In [4] we discussed the installation of the IN and OUT lines and the distribution and return lines that will go to each group of connectors. In principle the installation will happen this summer as they need to be passed from the gallery to the accelerator tunnel. Two options were discussed:

1. Having the gas rack in the Klystron Gallery and passing the 8 distribution + 8 return lines through the stubs to the accelerator tunnel
2. Having the gas rack in FEB-090 level and passing the 8 distribution + 8 return lines through the shielding wall to the accelerator tunnel

In Figure 16 we can see a sketch of the second option. It has the advantage to avoid the stubs and therefore the bending of the pipes needed through them. Second option is the preferred one by us and ESS, and is under discussion of implementation. In Figure 17 *Figure 16a* possible cylinder to pass the tubes through the shielding wall is shown. It is in fact as a patch panel. From there we can drive one pair of distribution+return line to each point of interest where we want to install a group of detectors. In the FEB-090 room we may want to have an extra patch panel between the wall and the rack depending on the final position of it.

In Figure 18 we can see the corresponding P&ID. The gas flows in parallel for the lines, therefore, if we want an operation flow of about 1l/h we need to have a flow from the bottle storage area of maximum slightly more than 8 l/h, depending on how many lines are in operation. At the entrance of each distribution line we will have an electrovalve as well as a pressure meter and a flowmeter connected in a control valve. At the return line there will also be an electrovalve and a flowmeter. Controlling the difference in the flow at the entrance and exit of a group of detectors we can be aware of possible leaks in this line and, in case needed, we can isolate it closing them. As mentioned before, all this equipment will be accessible at the level of the rack. In the diagram there are only 5 of each lines (5 distribution lines + 5 return lines) sketched, however, we will install 8 of each. From them, in principle, 5 will be used for the different groups of detectors plus 3 spares.

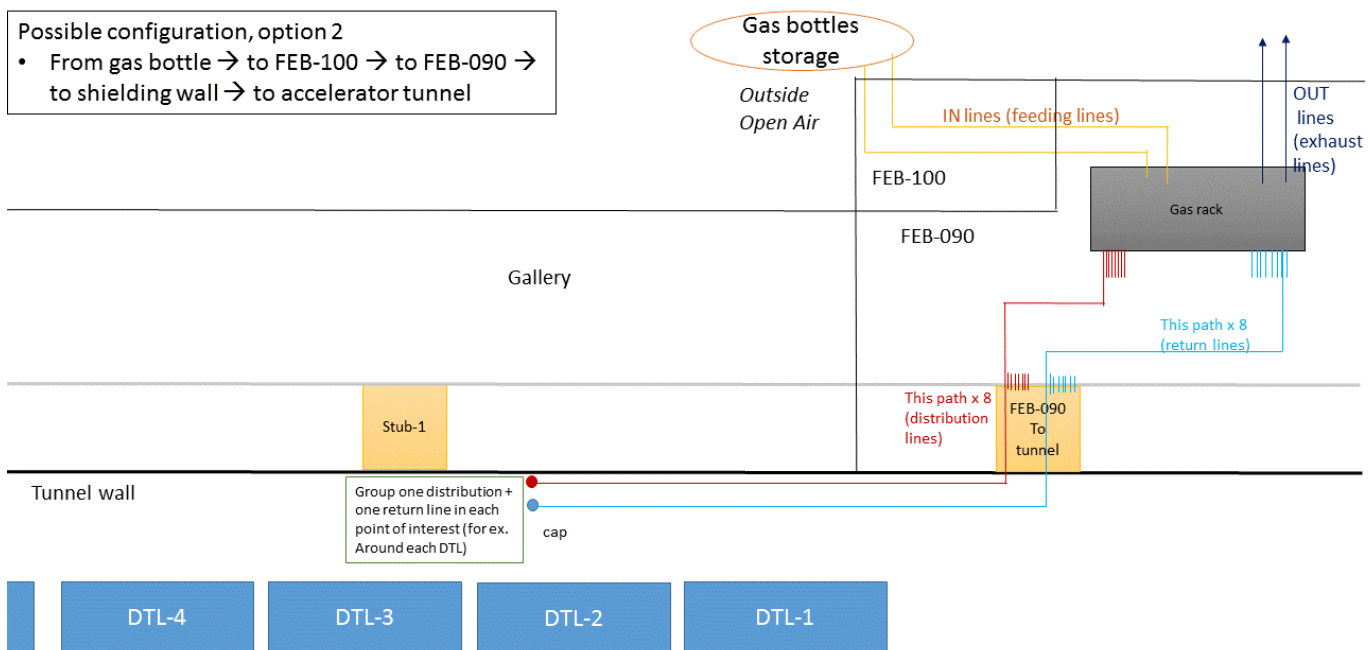


Figure 16: Sketch of the gas lines from gas bottles (outside building) into tunnel through the FEB-090. Only one distribution line + one return line path has been drawing through the FEB-090 shielding wall but 16 lines (8 distribution + 8 exhaust) need to be installed from the gallery to the accelerator. One distribution line + one return line is driven to each point of interest, i.e. to each group of detectors. Some lines will need to be driven another 500 m later to reach the spoke region. The lines passed through the shielding wall in room FEB-090 can be grouped inside a cylinder like shown in Figure 17.

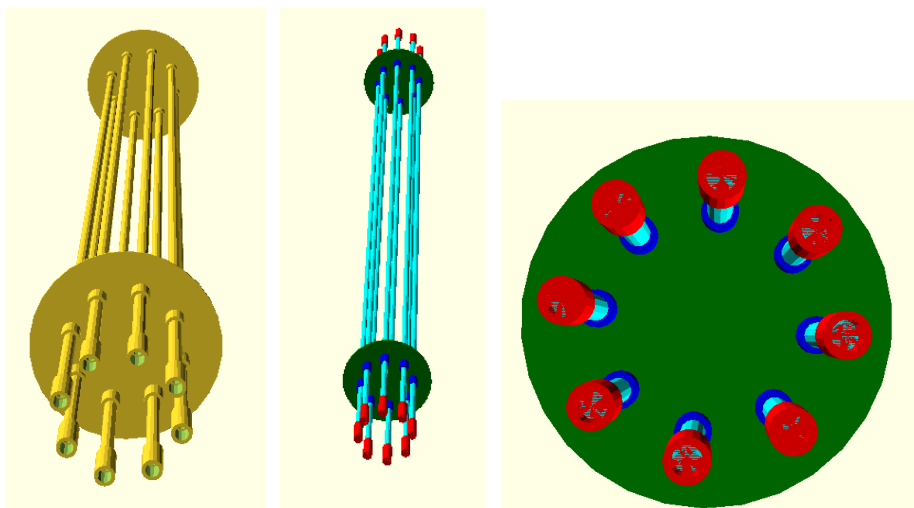


Figure 17: (Left) 3D drawings of possible passage through FEB-090 shielding wall. (Right) Front view of the pipes passage through the shielding concrete of FEB-090.

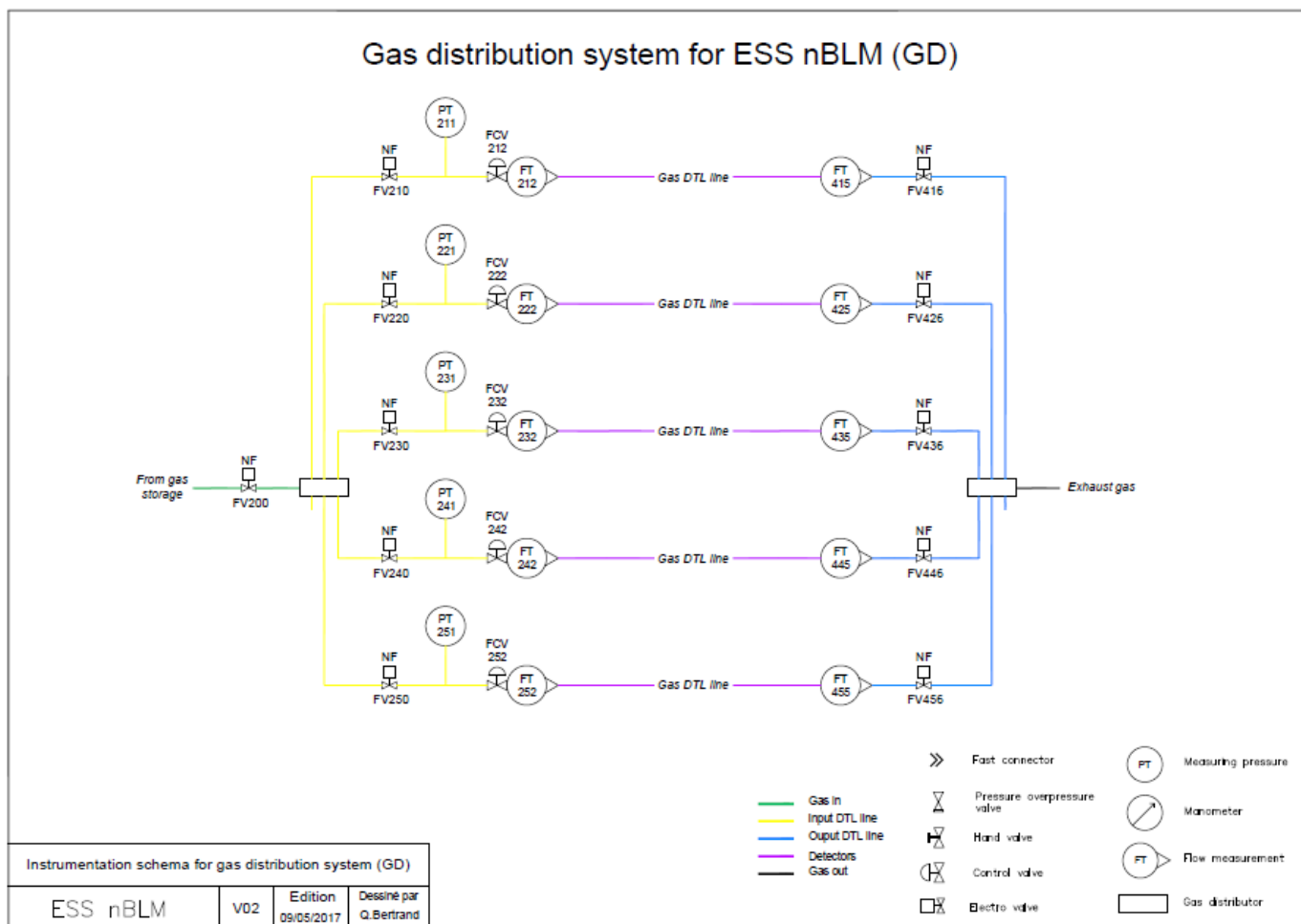




Figure 18: Gas distribution system for nBLM system. The distribution and return lines are sketched. In principle we will install 8 of each: 5 for the detector groups and 3 spares. Flowmeters at the entrance and exit of each line permit the control of leaks in each group of detectors and the electrovalves allow the isolation of one line without affecting the rest of the system in case of an intervention in one detector.

 	nBLM – PDR1.2	CEA-ESS-DIA-RP-0027
	ESS-I	Page 27 over 61

4.2.3. Gas line system for group of detectors

Each pair of distribution/return lines will feed several nBLM modules placed at a given location. They will be connected in series between them. The final distribution of the detectors needs to be decided to finalize this part of the system. A possible design with 10 modules (made by a slow and a fast detector each) around a DTL is shown in Figure 19. Each module can be isolated from the rest in case we need to do an intervention in the detector under consideration.

An intervention in a detector is expected in very few cases and will take place when the accelerator is OFF. There are two possible scenarios: one is when there is a leak in the line, determined by the drop in flow between the entrance and exit of the distribution line. This can only be studied with the accelerator OFF and in-situ. Another possible cause of intervention will be instability in one detector (high sparks rates or impossibility to reach the operational gains due to sparks). In this case we can switch off the voltages of this detector and not having it integrated in the system until a replacement can take place. For this reason we think it is interesting to have always 2 detectors covering more or less the same region in order to have redundancy.

For the replacement of a detector or mezzanine card we can isolate it from the rest manually for the intervention. The valve shown at the entrance of each detector is a shut-off coupler (Figure 20) that is closed automatically when disconnect from the line, therefore no air goes in and no gas goes out allowing also the exchange of detectors easier. In the P&ID we can see three possible options for the detectors connections. Another option will be to remove the extra tube and hand-valve, as the shut-off already closes the line when disconnecting the detector. In this case we can have prepared a little tube with two shut-off at each end to connect it in the place of the detector. So we can close the gas, remove the detector that we need to intervene on and connect the tube to open again the gas and have the rest of the detectors under recirculation.

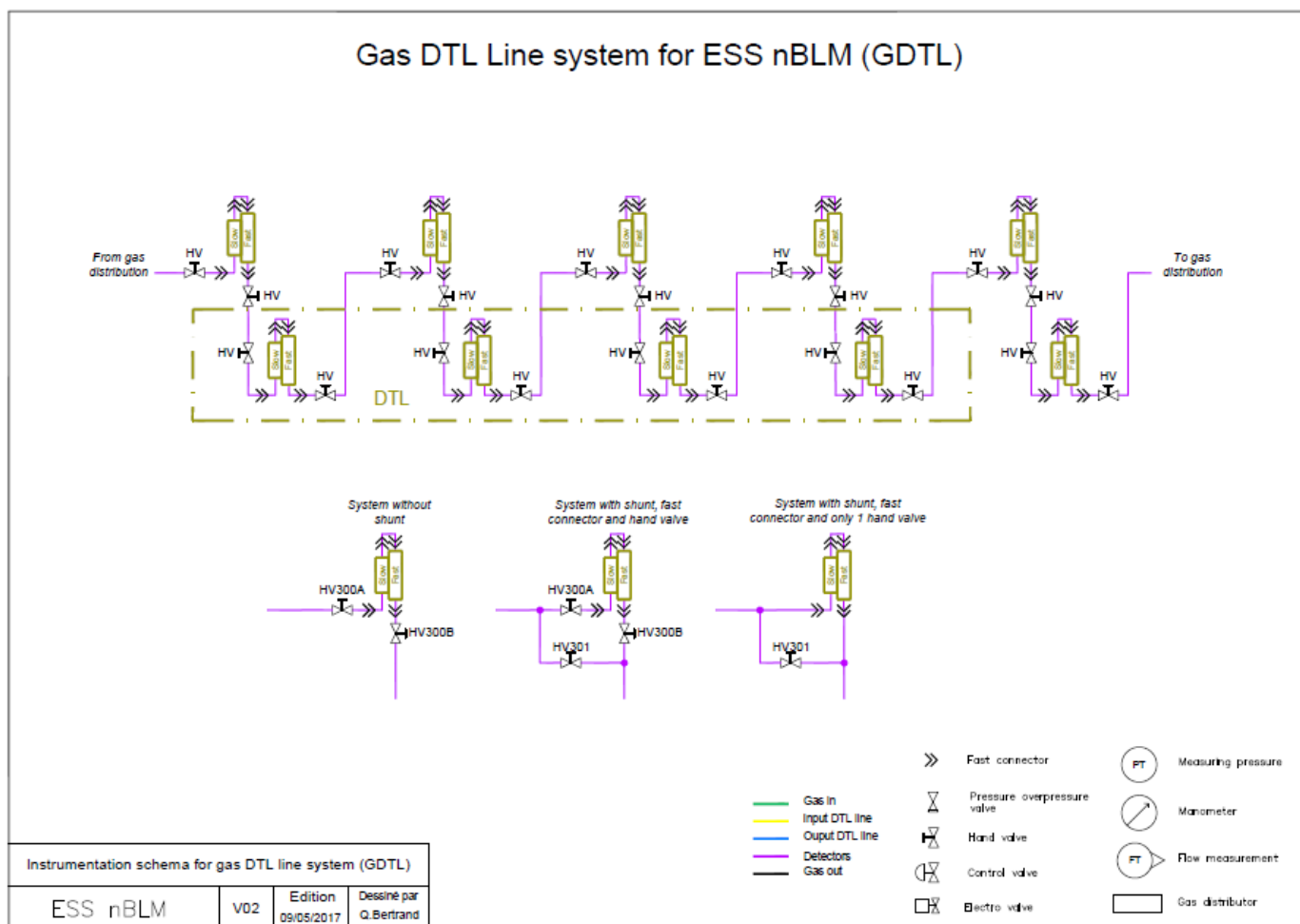


Figure 19: Gas line for a group of detectors, in this case around a DTL. 10 modules are shown, each one composed by a slow and a fast module. As we can see they are connected in series. Each one can be isolated from the rest by hand-valves when an intervention is needed.



Figure 20: Shut-off coupler to place at the entrance and exit of each nBLM detector to make easier their possible replacement and to avoid gas/air in and out during the operation.

4.2.4. Gas Rack and PLC controller

The gas rack will contain the hardware controller equipment and the control command subsystem in PLC. As an example we can show how this two elements look for a similar system designed by CEA/Saclay for CLASS12 (Figure 21). Both systems have the width of a 19" rack so can be integrated in one rack or can stand alone.

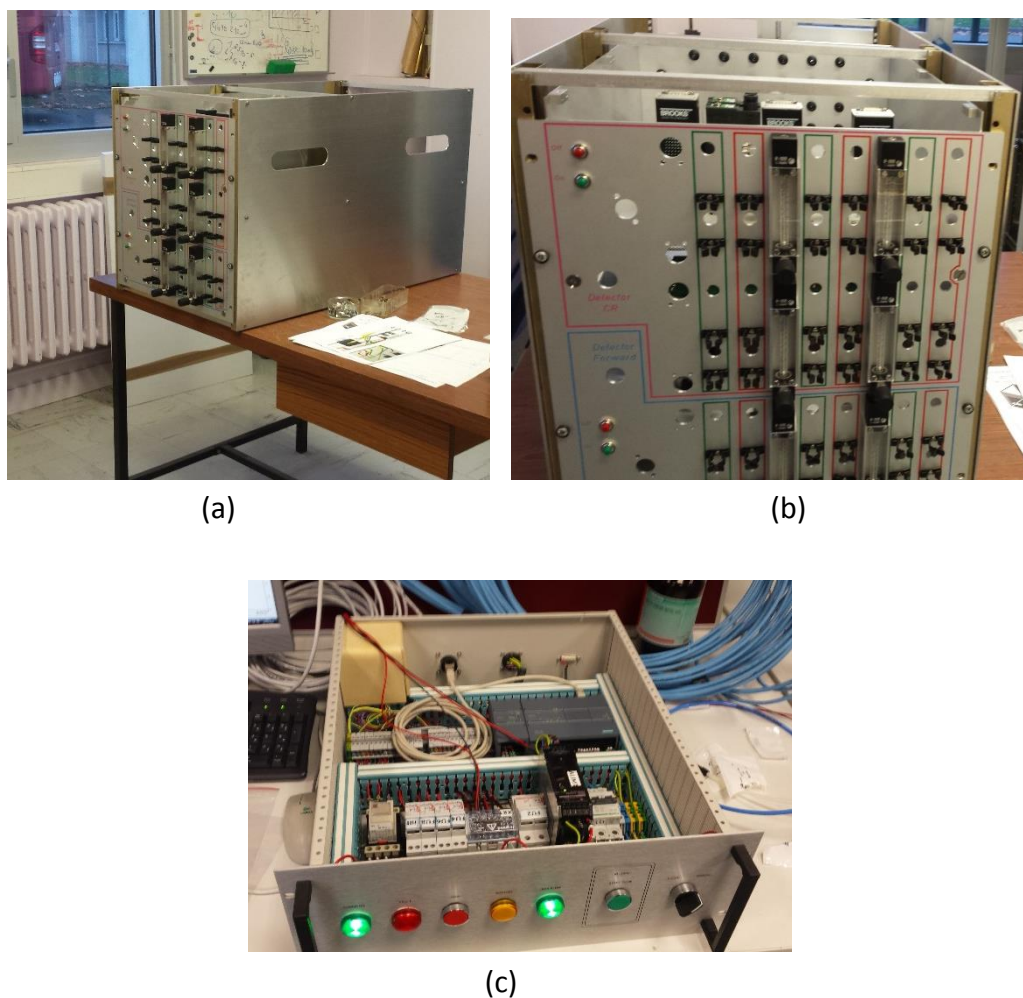





Figure 21: (a) and (b) example of a gas rack with the different control elements. In this case, the system was using bubble flowmeters also. (c) PLC system to control the different gas components.

 	nBLM – PDR1.2	CEA-ESS-DIA-RP-0027
	ESS-I	Page 30 over 61

4.3. List of components

We had a meeting the 1st of June with Duy Phan and Piero Valente to discuss about the selection of components. For the hardware the use of Swagelok is permitted and recommended. The components to use are listed in the following.

- Hand-valves
- Shut-off (fast connectors)
- Control valves
- Electro valves
- Pressuremeter
- Manometer
- Flowmeter
- Rotameter

	nBLM – PDR1.2	CEA-ESS-DIA-RP-0027
	ESS-I	Page 31 over 61

5. Control System

5.1. Requirements for the control

A nBLM module will consist of two Micromegas detectors. 42 modules will be delivered to ESS by January 2019. For the T5 baseline date (April 2018) ESS-I has to deliver a complete control system for one nBLM module prototype at Saclay including the gas control. This control system has to be a control template for the installation of the control of the nBLMs at Lund. The hardware and software developments will be compliant with ICS standards and follow ICS recommendations.

To be controlled, the nBLM needs a high voltage control. A fast acquisition around 250 MSamples per second is needed and the preamplifiers of the Front End Electronic require a slow control of low voltages.

5.2. Architecture overview

This architecture is compliant with the n-tier architecture described by ICS. The upper layer will consist of one PC dedicated to development and GUI displays. Another PC will be dedicated for the archiving Archiver Appliance.

The middle layer is dedicated to the EPICS servers or IOCs, it means the MTCA EPICS IOC for the fast acquisition and the Kontron (standardized by ICS) Industrial PC EPICS IOC for the PLC or CAEN slow controls. The overview of the system is shown in Figure 22.

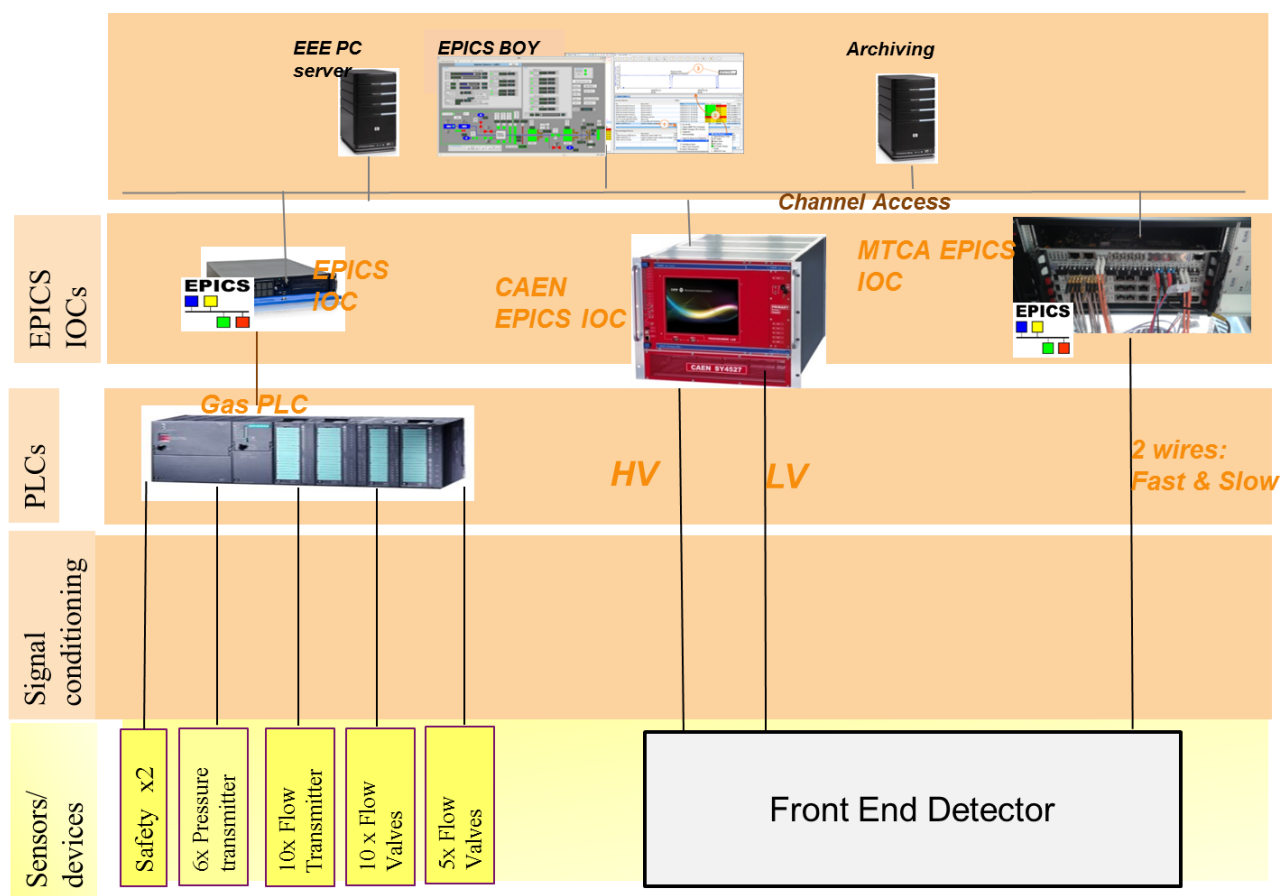


Figure 22: Architecture overview of the nBLM control system

5.3. Detector controls


5.3.1. CAEN High Voltages control

To control the high voltage, the CAEN SY4527 system has been chosen. In this system, A7030 modules will be plugged to control the Mesh and Drift voltages of each Micromegas detector. Each A7030 module can control 48 channels.

The CAEN A7030 provides the Universal Multichannel Power Supply System integrating an EPICS service that provides access to a Process Variable using the CA protocol. The EPICS IOC is integrated in the CPU of the crate. The CAEN SY4527 takes in charge its interlocks.

5.3.2. Low voltages control

To control the low voltage of the pre-amplifiers, CAEN A-2519 modules will be used and plugged on the same SY4527 crate.

	nBLM – PDR1.2	CEA-ESS-DIA-RP-0027
	ESS-I	Page 33 over 61

5.4. Fast acquisition

ICS standardisation for fast acquisition is based on MTCA.4, the IOxOS CPU IFC_1410 and IOxOS ADC_3111 FMC boards. IOxOS Technologies provides the IFC_1410, a MTCA.4 Intelligent FMC Carrier in AMC form factor featuring NXP PPC QorIQ processors of T Series and Kintex UltraScale FPGA devices. The IFC_1410 can carry 2 FMC boards ADC_3111.

5.5. FPGA software

The FPGA software development will take in charge the requirements presented in the document *“Requirements and functions to be implemented for the nBLM control system”* [3].

The FPGA will have 3 main tasks:

- Detection of neutrons and counting
- Trig an alarm on the Beam Interlock System if needed
- Supply of debug and diagnostic data (neutron rates ...)

The FPGA software design and development will be done by ESS ERIC.

5.6. System architecture at Saclay

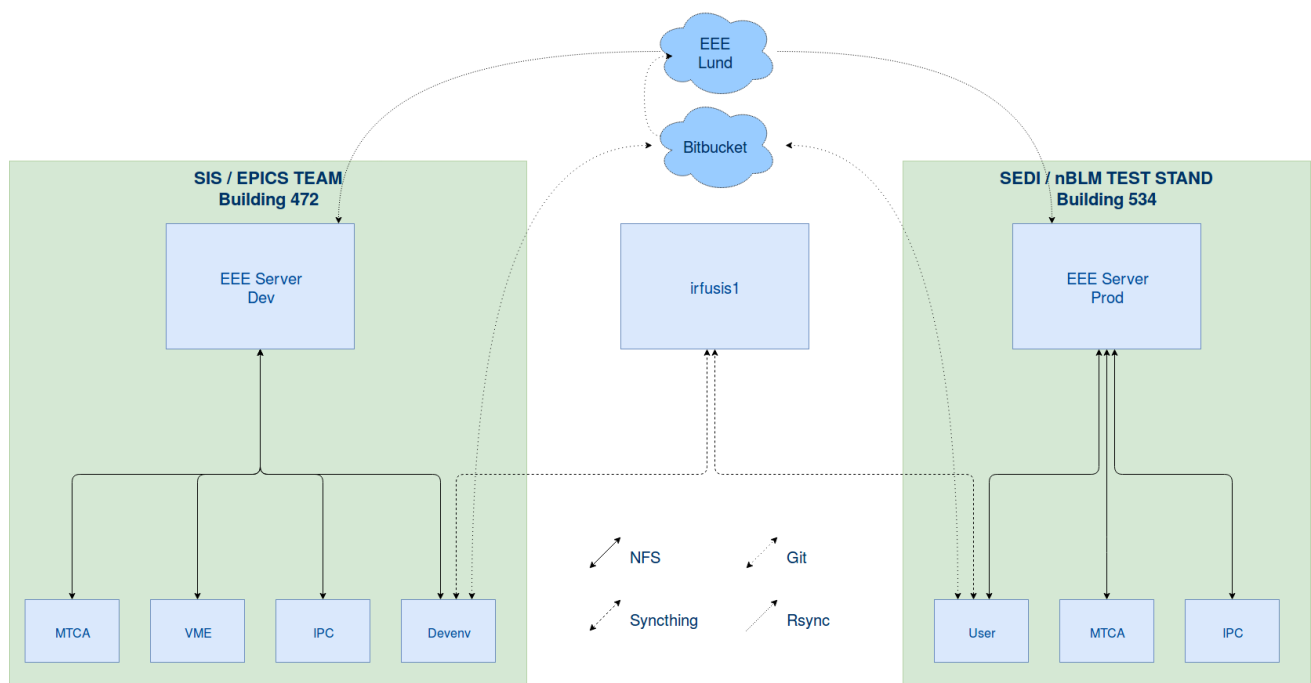



Figure 23: Software system architecture to be installed at Saclay

	nBLM – PDR1.2	CEA-ESS-DIA-RP-0027
	ESS-I	Page 34 over 61

A local area network will be installed at SEDI Laboratory for the nBLM prototype tests. This installation follows ICS recommendations. This LAN will include an EEE PC server. Another common PC will be dedicated to control tests with available GUI displays on the screen. This PC will also be used for possible software development updates.

5.7. Gas control

This section aims to provide a functional analysis of the gas control system for the nBLM system. It describes briefly the monitoring/PLCs/instrumentation architecture and presents the three subsets: Gas Storage (GS), Gas Distribution (GD) and Gas DTL Line (GDTL).

5.7.1. Gas control architecture

The hardware architecture complies with ESS standards and is shown in Figure 24. It consists of:

- Kontron Industrial PC with s7plc EPICS driver
- Siemens S7-1500 CPU
- Siemens Input/output cards

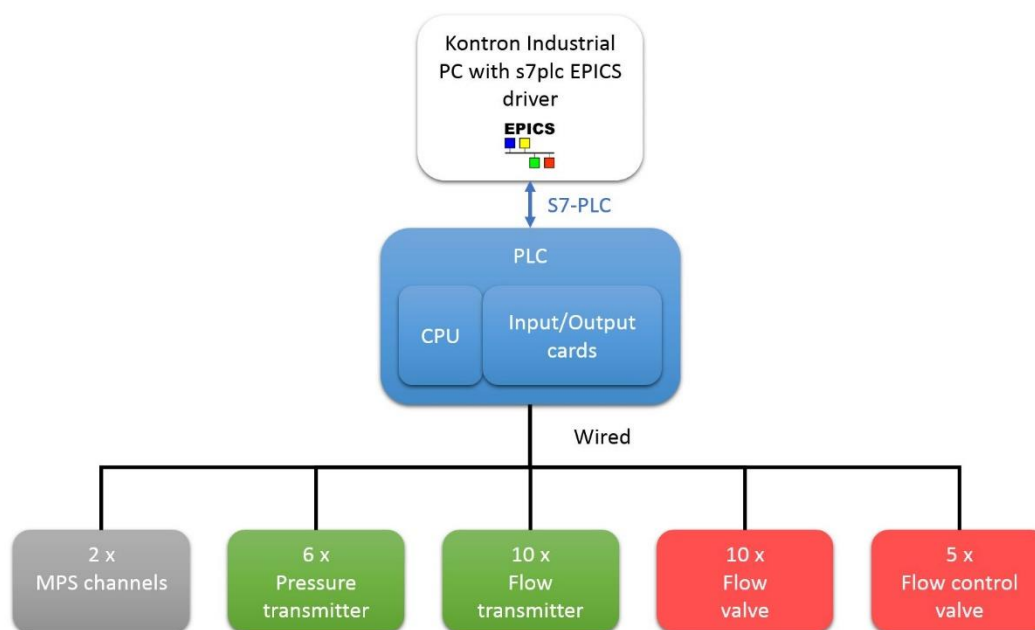



Figure 24: Gas control architecture

An EPICS server running on Siemens 1500 PLCs, developed by ESSi, communicates with the s7plc EPICS driver running on the Kontron industrial PC.

	nBLM – PDR1.2	CEA-ESS-DIA-RP-0027
	ESS-I	Page 35 over 61

Input cards acquire the pressure sensor values. Flow valves are controlled by digital output cards. Flow measurements and flow controls valves would be performed by Profibus Network. The PLC will manage the gas interlock.

A list of components has been proposed and it is attached to this document. In Figure 26 we can see an example of the power supply, the CPU and some of the cards, and how they will fit into a DIN-rail. We can also propose the option without Profibus, but we prefer its use to reduce the number of cards.

5.7.2. Gas control presentation

The main goal of the PLC is to ensure independently the integrity of the detectors. The PLC also manages the gas flow regulation. The PLC performs flow control (PID type) for each set of detectors. It will ensure the safety of the detectors with the control of the electrovalves. All the control settings and warning/fault thresholds can be fully adjusted by the user.

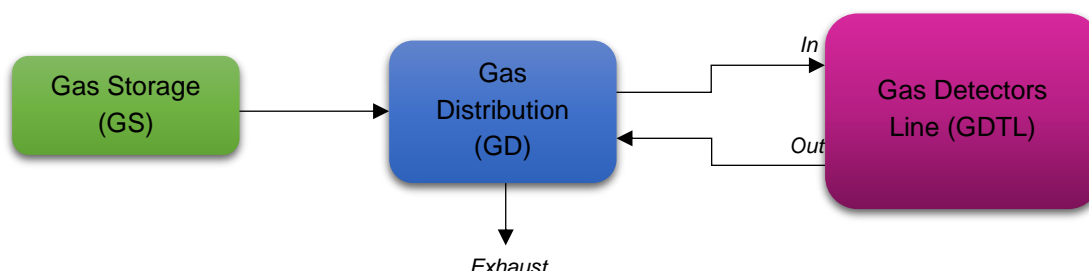


Figure 25: Gas system architecture



Figure 26: PLC system for the gas control example, with the CPU and Siemens cards connected.

6. nBLM distributed architecture

6.1. Detector position and racks

In [5] there is a table indicating the possible position of the nBLMs. In this section we discuss about this indication and how will impact the number of gas lines or acquisition cards. In section 7.4, a discussion about the results from simulations of different positions of the detectors in the DTLs is also presented.

The indications in [5] are:

- 5 nBLM modules in the MEBT section
- 11 in the DTLs sections
- 14 in the spokes sections
- 4 in the High β section

Note that the last two are with question marks in the document.

Regarding the signal acquisition, we should take into account that each ADC_3111 can read 8 channels. We have thought, that for the coincidence algorithms, it is better to try to group the detectors in similar sections. A possible configuration of the distribution and the racks to use is shown in Table 2. The racks have been chosen among the ones available for nBLM based on their location with respect the position of the detectors. The Figure 27 shows a graphical view of this table.

Rack name	Location	nBLM	ADC Channels	FMC	IFC	Spare	Comment
FEB-050	MEBT + DTL	5+4	18	3	2	6 channels	
SPK-010	DTL + spokes	7+7	28	4	2	4 channels	
SPK-050	Spokes	7	14	2	1	2 channels	>100 m separation between them
MBL-090	High β	4	8	1	1	0	

Table 2: Number of acquisition cards, IOCs and spare channels for the proposed distribution of detectors made in [5].

In conclusion, regarding the acquisition for the proposed 35 modules we need 10 FMCs card. However, for the 42 modules stated by the contract, we will need 11 FMCs. This could allow to separate the ones from the last spokes from the ones in the High β region if we think the distances for the cables are too long.

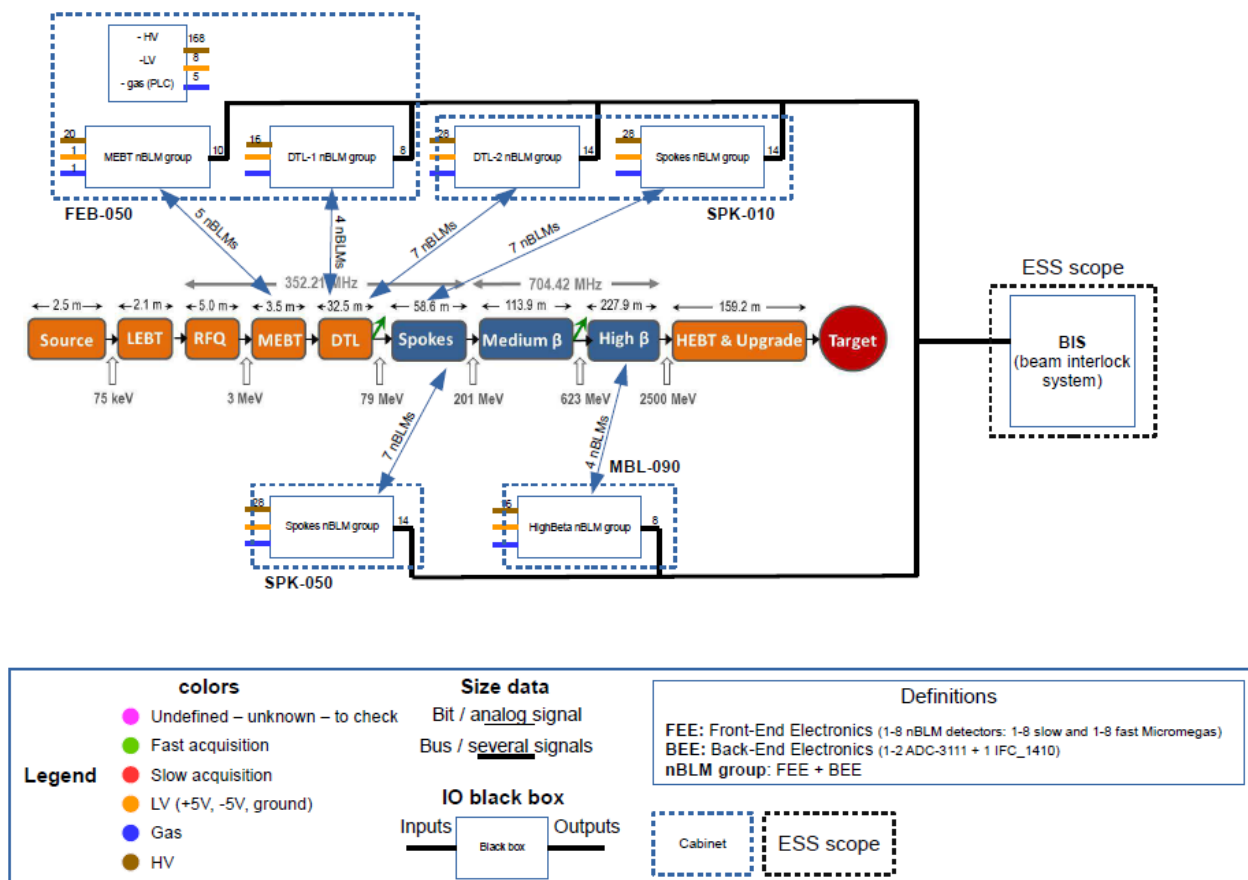


Figure 27: nBLM possible distributed architecture

Regarding the gas lines, we can group them in 5 groups:

- 3 groups for the MEBT and DTLs (5+11 modules): ~5modules/line
- 2 groups for the spokes and high β (14 + 4 modules): 9 modules /line approximatively

In any case it is very important that we fix the positions of the detectors for the decision on the racks and gas lines. Based on the simulations results shown in section 7 and in 7.4, in particular, in order to be able to say something about the location of the loss, we may need more than one detector per DTL. With more than one module per DTL we can compare the rates between them and help identifying the position of the loss with an accuracy given by the detectors separation. Therefore, depending on the regions where higher losses are expected, it would be more convenient to cover them with more detectors. In addition, due to the different expected rates between normal operation and the case of accidents, we may need very different operational settings. Therefore, some of the detectors need to be set for monitoring only and others for safety. Another question for the distribution is then if:

- We place the detectors individually (slow and fast separated) or
- We install the modules as a “whole”

HV and LV

As discussed in section 5, we have selected HV and LV modules from CAEN, which are inserted and give power by the SY-4527 B frame that can hold up to 16 extra cards. For the HV we will need 4 of them (48 channels/card). The 48 channels are read with a special cable (A648) that goes to SHV connectors. The module and cables' patch panel will be installed in the gallery in the rack. From there we can run the needed cables to the accelerator tunnel. Patch panels will also be installed in the tunnel. For the LV, in order to reduce cables, we plan to group the detectors. Assuming 5 groups of detectors, it implies 5 LV cables set ($\pm 5V$, GND). Therefore, with one card is enough (it has 8 outputs). We should assume one extra for spare. Therefore, with only a SY-4527 B frame we can power all the HV and LV modules needed for 42 modules.

However, some of the detectors will be placed in the spokes and high β regions, implying extra 312m of cable from first DTL if connected into same rack. For that reason, another possibility would be to have 2 SY-4527 B frames, one located in a rack in the region of the DTLs and another located in the region of the high energy. In Table 3 the budget needed for the use of just one SY-4527 B frame is shown. The installation of any extra one implies an extra cost of 6.21 k€.

In the case we use only one SY-4527 B frames, we have to take into account that we will need an extra power supply if we connect all the HV and LV modules, that costs 1.66 k€. However, this extra power supply also gives some extra security. For example, if the main power (A4531 that connects to the SY-4527 B) fails in the 48V used to feed the HV modules, there are the 48V provided by the A4533 that will continue to provide power to the boards. However, if the failure is in the 5V output, the CPU will stop working and so will the Main Frame. Therefore, it will depend on the failure of the main power supply. We need to discuss what the preferred option for ESS is.

Module	Price (€)	Number (baseline)	Total (k€)
SY-4527B	6.21	1	6.21
A7030N (HV)	5.37	4	21.48
R648 (HV cable)	1.53	4	6.14
A2519 (LV)	~5.0	2	10.0
A4533 (Extra double power supply for SY4527, 1200W)	1.66	1	1.66
Total			45.5

Table 3: Comparison of the prices for the two options discussed in the text to accommodate the HV and LV modules. Any extra SY-4527B module implies extra 6.21 k€.

6.2. Cables specifications and number


We can separate the cables in two parts: a first part connecting from the electronics rack in the gallery to the accelerator tunnel. They will be routing through the stubs to a patch panel. A second part goes from the accelerator tunnel patch panels to the detectors. The installation of the first part will happen soon and for this reason we have prepared and send a preliminary technical note [6] regarding the number of cables and their specifications in May 2017. In this section we summarized the discussion in there.

Each detector will have 3 connectors for the low voltage of the amplifiers ($\pm 5V$, GND), two high voltages connector (for the cathode and for the mesh), and, at least, one signal output. Therefore, for each one we will need 6 cables. However, as mentioned before, for the low voltage we can group the detectors and send one set from the rack to each patch panel, i.e, to each group. Once in the tunnel patch panel we will need to send one set of three LV cables individually to each detector.

In Table 4, the number of cables for the first installation (from Klystron gallery to accelerator tunnel) for the baseline of the system, i.e., one signal cable per detector, is summarized. The specifications of each cable is also indicated. All of them have been chosen from the ESS database and are already approved by ESS. We list enough cables for 42 modules plus another 40 extra HV cables that implies the possibility to install 10 extra modules. Therefore spare signals cables (30) will also be needed. For the LV we need 3 long ones (from gallery) to each patch panel. The installation of 8 patch panels is proposed. We also propose that each patch panel serves for 10 nBLM module, i.e. for 20 detectors, to account also for spare connectors. For the routing of the last part (from tunnel accelerator patch panel to detectors) we need to decide the positions and how many will be in each area.

		Number		
Cable type	Specifications	Per detector	Spare	Total
HV cables	1C20 RG 58 HV	2	40 (10 modules)	208
Signal	1CRG-174 HF	1	30 (15 modules)	114
Cable type	Specifications	Per patch panel	Spare	Total
LV	$\pm 5V$	2	2	32
	GND	1	1	16

Table 4: Specifications for each kind of cable needed per detector. All of them are already approved in the ESS cable database. The total number of cables proposed for installation is also listed.

	nBLM – PDR1.2	CEA-ESS-DIA-RP-0027
	ESS-I	Page 40 over 61

7. Response to ESS scenarios

The new results regarding the MonteCarlo studies of the nBLM modules response and geometry are shown in document [1]. In this document we highlight the main results but refer to this document for further details. Also for the studies regarding the optimization of the design and the first prototype design details, we refer to the PDR1.1 [7].

In [7] the response of the nBLM detectors under different accidental scenarios simulated by the BI-ESS and explained in [5] was shown. In this document, more accidentals scenarios are studied as well as the 1% 1W/m scenario. In addition, the results for different locations of the detectors are shown. Also we discuss about the threshold between “thermal” and fast neutrons. Regarding the detector design, after the PDR1.1, it was decided not to use Cd as thermal neutron absorber but a borated rubber. Results from MonteCarlo simulations with this material are also discussed here.

7.1. Response for 1% 1 W/m losses compared with accidents

In order to accomplish with the nBLM system requirements, it needs to be sensitive to losses of 1% of 1W/m within the required time response (5 μ s total, 3 μ s for the detector + FEE response). These have been studied through MonteCarlo simulations of the nBLM response under ESS simulated scenarios provided by ESS. As explained in [7], ESS provide us with the list of produced particles in each loss scenario simulated. This list of particles with their properties (energy, momentum, time, etc....) is the input in our nBLM-Geant4 simulation framework to study the response of the nBLM slow and fast detector.

Different strategies have been discussed with ESS. One option, and the one that seems the most reliable one, is to scale down the simulated scenarios of localized losses, or accidents, to the case of 1% 1W/m loss. In addition, two other loss scenarios were simulated and explained in [5]: one corresponding to the normal loss scenario taking into account the beam dynamics, and the other a uniform loss scenario. In document [1] the rates obtained in the three cases and the details of the assumptions done are explained. Here, only the results for the scaling down of the accidents are shown. The reason why we consider it the best approximation is that, in this case, we know the number and energy of protons producing the loss and that it is a localized one. In the other two cases, we have made two assumptions: one is that the initial number of simulated protons was evenly distributed along the 5 DTLs, and the other assumption, is to assume that only the protons produced in the region where the detector is located contributed to the detected loss. In that sense, we are underestimating the expected number of particles. This assumption was done as we don't have information about the initial protons distribution.

The provided accidental scenarios correspond to 13 files where the loss is produced at different locations at, either the DTL-1 or the DTL-5. In addition, some of them corresponds to the same simulation but varying some parameters. They are listed in Appendix 1. In Table 5 we show the list of files used and some of their characteristics. These files have been used to obtain the expected rates in the nBLM in case of accident and also to scale them down for the mentioned cases of 1% 1W/m.

ESS file	Loss location	Proton Energy (MeV)	Protons simulated	Bunches simulated	Neutrons produced in scenario	N's/ bunch	Comments
sim2-0	Mid DTL-1	11.5	6.00E+08	5.45E-01	2.90E+05	5.31E+05	Max θ in DTL1, 50mrad, $\sigma_{xy} = 1\text{mm}$
sim2-1	$\frac{3}{4}$ DTL-1	17.9	1.00E+08	9.09E-02	2.33E+05	2.56E+06	Max θ in DTL1, 50mrad, $\sigma_{xy} = 1\text{mm}$
sim2-3	Mid DTL-1	11.5	6.00E+08	5.45E-01	2.86E+05	5.24E+05	Same as sim2-0 but $\varphi = -90^\circ$, $\sigma_{xy} = 1\text{mm}$
sim2-8	Start DTL-5	71.8	4.00E+07	3.64E-02	4.33E+06	1.19E+08	Max θ in DTL5 10 mrad, $\sigma_{xy} = 0$
sim2-11	End DTL-5	86.5	4.00E+07	3.64E-02	4.38E+06	1.20E+08	Max θ in DTL5 10 mrad, $\sigma_{xy} = 1\text{mm}$
sim2-12	End DTL-5	86.5	4.00E+07	3.64E-02	3.94E+06	1.08E+08	Same as sim2-11 but $\sigma_{xy} = 0$
sim2-13	Mid DTL-5	79.3	4.00E+07	3.64E-02	3.94E+06	1.08E+08	Max θ in DTL5 10 mrad, $\sigma_{xy} = 0$

Table 5: List of ESS files used as the input in the nBLM-Geant4 simulation. Some of their characteristics like energy or incident angle are shown, as well as the number of neutrons produced per scenario.

In the nBLM simulation, in which we use as input the different ESS files, the detectors have been placed around the DTL where the lost is produced in the same reference system as the one in the ESS simulations. Following the recommendations done in [5], they are placed at 0, $\frac{1}{4}$, $\frac{2}{4}$ and $\frac{3}{4}$ of the DTL length along the beam direction, as sketched in Figure 28. Therefore, for each scenario we have simulated 4 different nBLM located at these positions of the corresponding DTL. In the following, the detectors are labelled as det1 at 0z, det2 at $\frac{1}{4}z$, det3 in the middle and det4 at $\frac{3}{4}$ of z. Most of the studies have been done placing them on top of the linac, i.e. at $x=0$ and at y fix to 65 cm. The positions are summarized in Table 6. The initial particles are sampled from the ESS files, i.e. their momentum, energy and position are used. Once they enter in the nBLM detector they are saved if they deposit energy in the gas volume. We save the initial and deposited energy, the global time of the particle, and their position. A visualization of the nBLM-G4 simulation is shown in Figure 29.

DTL-1	Position (cm)						
	x	y	z	DTL-5	x	y	z
det 1	0	65	-2649	det 1	0	65	465
det 2	0	65	-2455	det 2	0	65	665
det 3	0	65	-2261	det 3	0	65	865
det 4	0	65	-2067	det 4	0	65	1065

Table 6: Position of the nBLM detectors in the G4-nBLM simulations carried out using the ESS data as input. Four detectors have been placed on top of the linac along the z-axis of the DTL-1 and DTL-5 to study their response to the simulated losses scenarios. They have been placed with respect to the input file reference system.

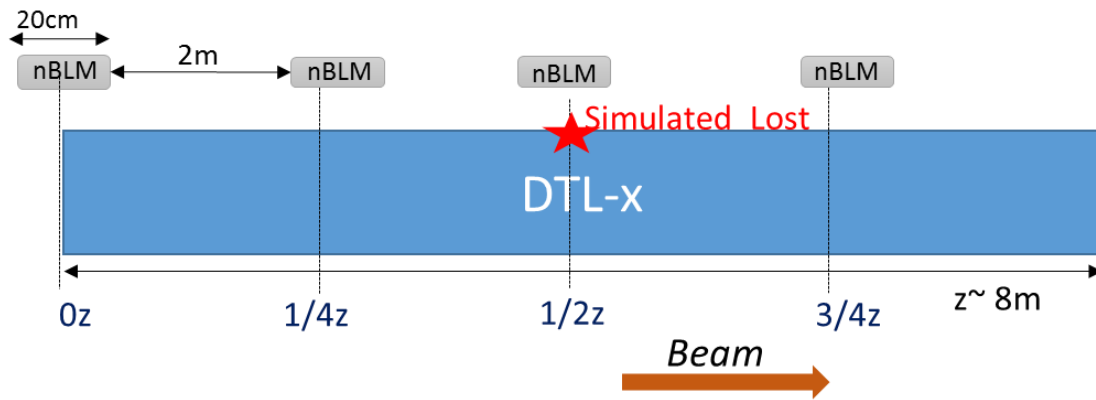


Figure 28: Schematics of the position of the nBLM around the DTL. The separation between each detector is $\sim 2\text{m}$. In the following, they are labelled as det1 at $0z$, det2 at $1/4z$, det3 in the middle and det4 at $3/4$ of z in the direction of the beam. The loss is produced in a location in the case of accidental losses. In most of the results presented here the modules have been placed on top of the accelerator at 65cm from the beam centre. In other cases discussed later they are placed on the lateral at a same distance or in the middle between two DTLs.

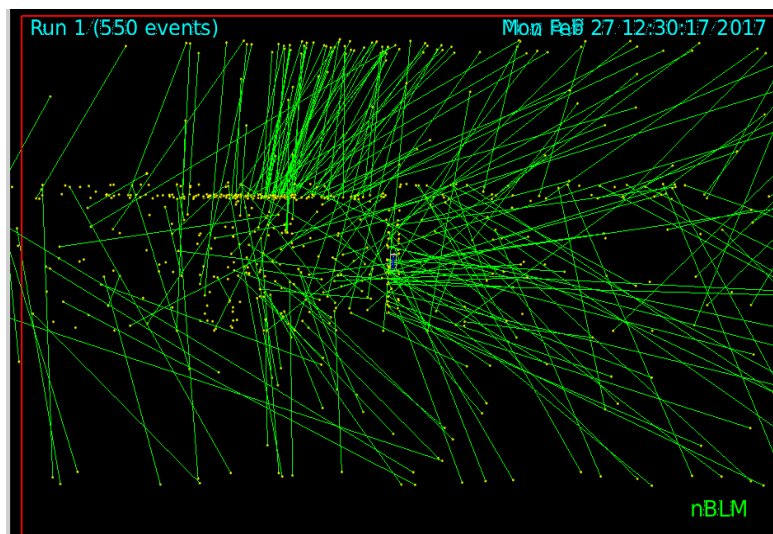


Figure 29: Geant4 visualization. (Left) Tracks of the neutrons used as our input: the neutrons produced in the case of an accidental loss at $1/4$ of DTL-5. The structure of two consecutive DTLs can be viewed. In this case the detector was placed between the two linacs (in blue).

In all the cases, the number of neutrons simulated in the nBLM-G4 run corresponds to more than one bunch, and the number of counts detected has a statistical relative error of $\sim 1.5\%$ in the cases of the slow detector simulations. The number of simulated events in each case is listed in Table 7.


Input	DTL	Simulated number of neutrons ($\times 10^8$)			
		det0	det1	det2	det3
sim2-0-DTL	1	5.5	5.5	21.5	21.5
sim2-1-DTL	1	11	11	11	11
sim2-3-DTL	1	11	11	11	11
sim2-8-DTL	5	11	11	11	11
sim2-11-DTL	5	11	11	11	11
sim2-12-DTL	5	11	11	11	11
sim2-13-DTL	5	11.0	1.72	2.2	2.75

Table 7: Number of simulated neutrons for each of the nBLM “first module” detectors placed around the DTL-1 and DTL-5 for the different ESS input files used.

The rates are calculated as following, explained in [1] and [7]. Every neutron that deposit energy in the nBLM is recorded and saved for later analysis. In the analysis, we only take into account the events that deposit an energy > 10 keV in the detector. The electronics and electric field are not simulated, however, due to the small drift volume we can assume that any particle depositing energy inside the gas volume will be detected.

The two most relevant magnitudes are the expected rates and the time response. The time response was largely studied in [7], so it will not be treated in this document. The expected rate was also studied for different accidental cases but more cases are discussed here. In addition, the expected rates in the case of 1% 1W/m loss case are obtained.

In Table 8 we summarized the rates for the case of accidents detected in the slow module. The number of detected events are listed, with its statistical error, for each scenario. Then the c/bunch was calculated taking into account how many bunches we have simulated. To obtain the number of bunches simulated we use the information from the simulated number of protons and how many neutrons have been produced in the ESS scenario. Then, normalizing for the number of protons per bunch, we can obtain the expected number of neutrons produced per bunch in the given scenario. In order to calculate how many events are detected within a time (in this case after the first and third μs) we have to take into account that the frequency of the detector is shorter than the time response of the slow nBLM detector (100% of the events are detected in $\sim 200 \mu\text{s}$ in the slow module). We will start detecting events from the second bunch before all of the 1st bunch have been detected. The

	nBLM – PDR1.2	CEA-ESS-DIA-RP-0027
	ESS-I	Page 44 over 61

values are listed in the last two columns. As it can be seen the rates range from 10 MHz in the low energy region up to 50 GHz in the high energy region after 1 μ s.

In addition, data is plotted along the z-axis¹ in Figure 30. We can see that some information about the location of the loss can be obtained with an accuracy depending on the detector size and detectors separation. Also, from the data we can conclude that there is not a significant difference if we consider a Gaussian beam (RMS ~ 1 as explained in [5]) or a pencil-like beam profile if the detector is placed on top of the loss (compare results from files sim2_11 and sim2_12). However, for the detectors located far away from the loss, the rates decrease in the case of a pencil-like beam scenario compare with the Gaussian case, a factor about 1.5.

Lowest and highest estimated high rate

The other special case, is to compare scenarios sim2_0 and sim2_3. The difference between them is that in sim2_3 the beam azimuthal angle is -90° , pointing away from the nBLM volume (DTL1-det1), while sim2_0 points towards the DTL1-det2, as indicated in [5]. The comparison can give an estimation of the difference between the highest and lowest expected rate in case of an accident (as suggested in [5]). Results obtained are the same within $\sim 2\sigma$ maximum in both cases. Same result is obtained placing the detector in the lateral as in [1].

¹ The positions are relative to the ESS simulation reference system, being approximately: DTL1 between [-2639,-1863]cm, DTL2 between [-1853,-1133]cm, DTL3 between [-1123,-349]cm, DTL4 between [-339,+465]cm, DTL5 between [+475, +1276]cm.

ESS input	nBLM	Bunches simulated	Counts detected	c /bunch	c in the first μ s (MHz)	c in the first 3 μ s
sim2-0 <i>midDTL-1</i>	det1	1035.78	0	---	---	---
	det2	1035.78	1765 ± 42	1.70 ± 0.04	16.70 ± 4.09	117.24 ± 10.83
	det3	4048.96	33163 ± 1734	7.45 ± 0.04	59.81 ± 7.73	433.50 ± 20.82
	det4	4048.96	12985 ± 114	3.21 ± 0.03	13.82 ± 3.72	118.65 ± 10.89
sim2-1 <i>3/4 DTL-1</i>	det1	429.69	0	---	---	---
	det2	429.69	532 ± 23	1.24 ± 0.05	7.20 ± 2.68	57.26 ± 7.57
	det3	429.69	1780 ± 42	4.14 ± 0.10	28.60 ± 5.35	218.81 ± 14.79
	det4	429.69	4970 ± 50	11.57 ± 0.16	80.76 ± 8.99	665.61 ± 25.80
sim2-3 <i>midDTL-1</i>	det1	2099.24	0	---	---	---
	det2	2099.24	3310 ± 58	1.58 ± 0.03	8.21 ± 2.87	8.21 ± 2.87
	det3	2099.24	12646 ± 112	6.02 ± 0.05	54.28 ± 7.37	54.28 ± 7.37
	det4	2099.24	6192 ± 79	2.95 ± 0.04	16.64 ± 4.08	16.64 ± 4.08
sim2-8 <i>startDTL-5</i>	det1	9.24	25824 ± 161	2793.69 ± 17.38	26830.00 ± 163.80	175838.00 ± 419.33
	det2	9.24	7542 ± 87	815.91 ± 9.40	5974.00 ± 77.29	41318 ± 203.27
	det3	9.24	3784 ± 82	409.36 ± 6.65	2021.00 ± 44.96	16479.00 ± 128.37
	det4	9.24	2388 ± 49	258.34 ± 5.29	608.20 ± 24.66	8458.90 ± 91.97
sim2-11 <i>endDTL-5</i>	det1	9.17	2880 ± 54	314.18 ± 5.85	1392.00 ± 37.31	12928.90 ± 113.71
	det2	9.17	3080 ± 56	336.00 ± 6.05	1418.00 ± 37.66	12111.80 ± 110.05
	det3	9.17	5494 ± 74	599.35 ± 8.09	2557.00 ± 50.57	23912.40 ± 154.64
	det4	9.17	10768 ± 104	1174.69 ± 11.32	7504 ± 86.63	58655.90 ± 242.19
sim2-12 <i>endDTL-5</i>	det1	10.19	2612 ± 51	256.45 ± 5.02	875.50 ± 29.61	7709.00 ± 87.80
	det2	10.19	3440 ± 59	337.75 ± 5.76	954.50 ± 30.89	9395.00 ± 96.93
	det3	10.19	5158 ± 72	506.42 ± 7.05	2328.00 ± 48.25	19971.10 ± 141.32
	det4	10.19	11334 ± 106	1112.79 ± 10.45	5300.00 ± 72.80	47375.00 ± 217.66

sim2-13 midDTL-5	det1	10.19	5403 ± 74	530.48 ± 7.22	2545.03 ± 50.45	20073.70 ± 141.68
	det2	1.07	889 ± 30	827.69 ± 27.76	4518.26 ± 67.22	36455.10 ± 190.93
	det3	2.04	7656 ± 87	3758.40 ± 42.95	51790.90 ± 227.58	302911.00 ± 550.37
	det4	2.04	1568 ± 40	769.65 ± 19.44	4914.98 ± 70.11	37477.80 ± 193.59

Table 8: Number of counts detected in each nBLM slow module for each scenario simulated. Also listed are the counts per bunch and number of counts after the first 1 μ s and 3 μ s after the accident happens. Errors are statistical errors.

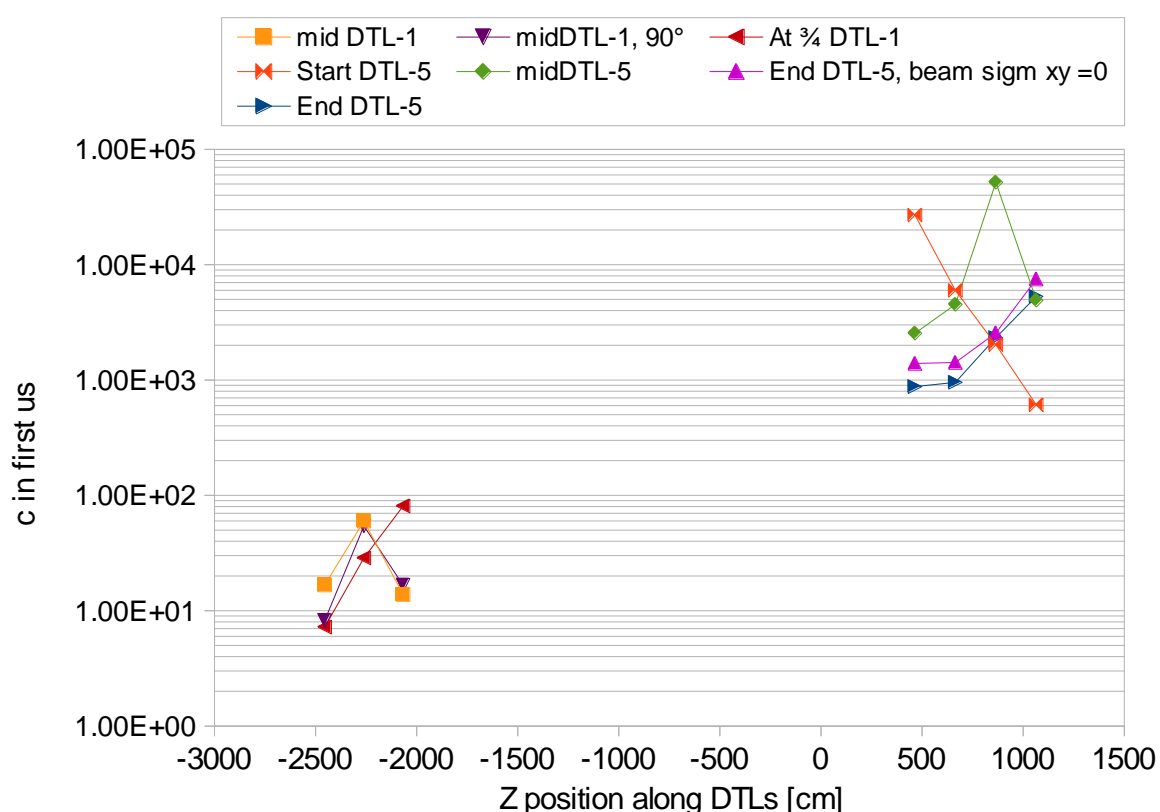


Figure 30: Rate detected in the nBLM slow detectors placed at different locations along the beam axis and for different lost scenarios provided by the ESS. The detectors are placed more exactly around DTL-1 and DTL-5. The rate has been computed after the first μ s after the accident.

Now, we can use the accidental cases to scale to the 1% 1W/m loss case. The advantage of using the accidental scenarios is that we have a loss occurring in a clear location with a known number of protons with a fixed energy. Therefore, we can calculate the produced power, and used it to normalize the counts detected in the nBLM to the desired case. We assume it is lost in 1 meter. Then, we normalize for the considered active time. For example, we can assume if the lost is loss along one

pulse (2.86 ms duration) or along the duty cycle (14*2.86ms). Concretely, as explained in [1], the normalization is:

$$C_{det} \cdot \frac{N_N}{N_N^{Simu}} \cdot \frac{1W/m}{x W/m} \cdot \frac{1}{\text{Active Time}} \quad \text{Eq. 1}$$

where c_{det} is the events detected in the nBLM, N_N is the number of neutrons produced in the corresponding BI-ESS scenario (listed in Table 5), N_N^{simu} is the number of simulated neutrons by us (Table 7) and x is the calculated power emitted in these scenario (listed in Table 9). In Table 10 we show the counts after normalization and the rate expected if the loss is uniformly (in 14 Hz) and taking into account the 1% of 1W/m. We compare this values with the accidental rates in Figure 31. A factor between 3.5×10^4 and 7.7×10^5 of difference is expected in the rates, assuming all the lost occurs uniformly. That means, rates of 0.1 kHz to 68 kHz (100c/s to 68000c/s, in the low and high energy region respectively).

ESS Input	Position of the loss	Ep (MeV)	Ep (J)	N _p	W/m/s
sim2-0-DTL	Mid DTL-1	11.5	1.84×10^{-12}	6.00×10^8	1.10×10^{-3}
sim2-1-DTL	¾ DTL-1	17.9	2.86×10^{-12}	1.00×10^8	2.86×10^{-4}
sim2-3-DTL	Mid DTL-1	11.5	1.84×10^{-12}	6.00×10^8	1.10×10^3
sim2-8-DTL	Start DTL-5	71.8	1.15×10^{-11}	4.00×10^7	4.60×10^4
sim2-11-DTL	End DTL-5	86.5	1.38×10^{-11}	4.00×10^7	5.54×10^4
sim2-12-DTL	End DTL-5	86.5	1.38×10^{-11}	4.00×10^7	5.54×10^4
sim2-13-DTL	Mid DTL-1	79.0	1.26×10^{-11}	4.00×10^7	5.06×10^4

Table 9: Lost produced in W/m/s in each of the accidental losses scenarios simulated.

1% 1W/m uniformly in 14 Hz						
ESS input	nBLM	c/ms (kHz)		ESS input	nBLM	c/ms (kHz)
sim2-0 (mid DTL-1)	det1	---		sim2-11 (end DTL-5)	det1	5.17 ± 0.10
	det2	0.21 ± 0.01			det2	5.53 ± 0.10
	det3	0.92 ± 0.01			det3	9.87 ± 0.13
	det4	0.396 ± 0.003			det4	19.34 ± 0.19
sim2-1 (¾ DTL1)	det1	---		sim2-12 (end DTL-5)	det1	4.22 ± 0.08
	det2	0.098 ± 0.004			det2	5.56 ± 0.10
	det3	0.33 ± 0.01			det3	8.34 ± 0.12
	det4	0.92 ± 0.01			det4	18.31 ± 0.17
sim2-3 (mid DTL1)	det1	---		sim2-13 (mid DTL-5)	det1	9.56 ± 0.13
	det2	0.195 ± 0.003			det2	14.92 ± 0.50
	det3	0.74 ± 0.01			det3	67.73 ± 0.78
	det4	0.364 ± 0.005			det4	13.87 ± 0.35
sim2-8 (start DTL-5)	det1	55.25 ± 0.35				
	det2	16.14 ± 0.19				
	det3	8.09 ± 0.13				
	det4	5.10 ± 0.11				

Table 10: Rates obtained for the nBLM slow modules in each accidental scenario simulated but normalizing to the case of 1% 1W/m, and distributed uniformly in 14Hz, as explained in the text.

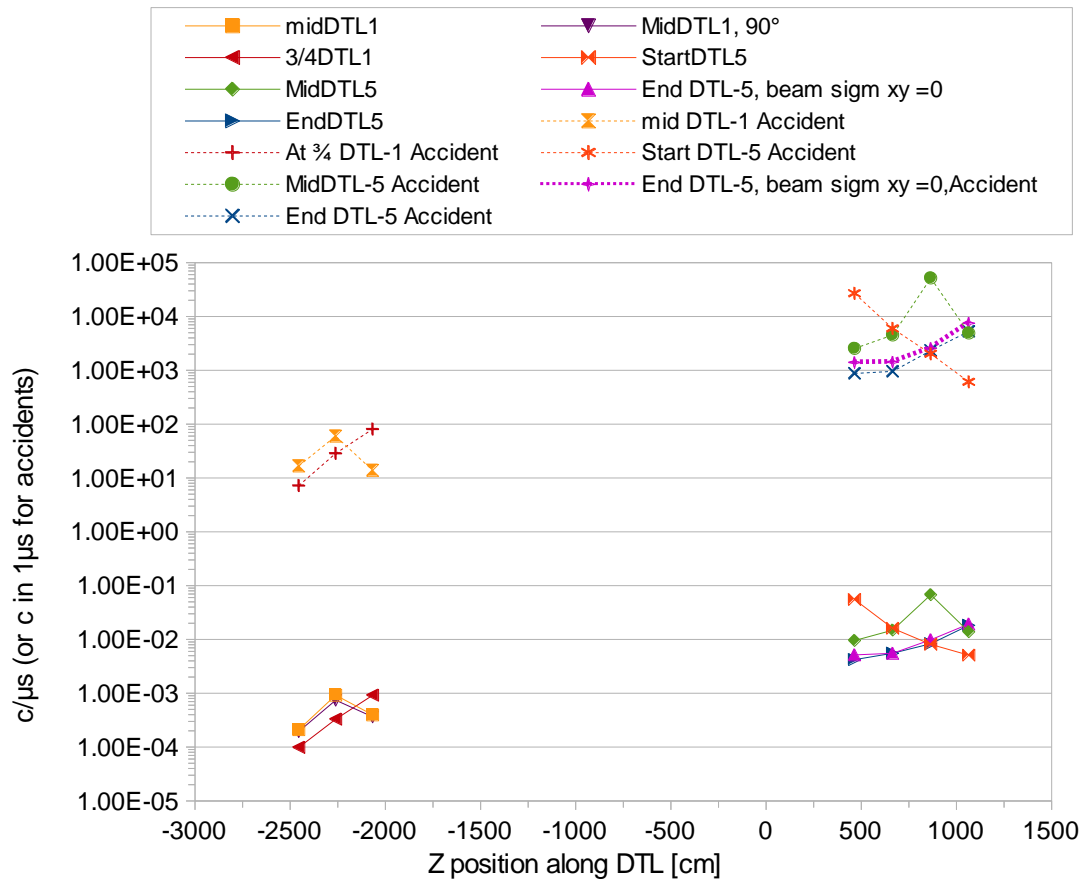


Figure 31: Comparison between the rates obtained in case of accidents (dashed lines) with respect normalizing them to 1W/m loss (solid lines). They have been computed for different loss scenarios in which the nBLM slow detectors have been placed at different location around DTL-1 and DTL-5 (x-axis).

7.1.1. Fast module

In Table 11 we show the rates detected for the same scenarios in the fast module. In this case, as the response is of ~ 10 ns, all the events from the first bunch are detected within the needed response time. The accidents were also used to calculate the expected rates detected in case of 1% 1W/m loss as in the case of the slow module, this is shown in Table 12. Also in Table 12 the case of the accidents are listed together with the 1% 1W/m case for easier comparison. As before, the rates are plotted versus their position along the beam axis in Figure 32. As explained in [1] only the detectors with enough statistics have been used for the calculations. In case of 1% 1W/m loss the rates range between 2.5 Hz to 1.5 kHz (2c/s and ~ 1500 c/s), at the low and high energy regions respectively. As in the case of the slow modules there is a clear difference between rates at normal operation and in case of accidents. In this case it is a factor about 3×10^5 and 3×10^7 .

ESS input	nBLM detector	Bunches simulated	Counts detected	c/bunch	c/μs (MHz)
sim2-0-DTL	det3	1224.11	78 ± 9	0.060 ± 0.007	22.44 ± 2.54
sim2-1-DTL	det3	859.38	26 ± 5	0.030 ± 0.005	10.65 ± 2.09
sim2-8-DTL	det1	18.49	975 ± 31	52.70 ± 1.69	18569.94 ± 594.71
	det2	18.49	26 ± 5	1.41 ± 0.28	495.20 ± 97.12
sim2-11-DTL	det3	36.67	34 ± 6	0.93 ± 0.16	326.50 ± 56.00
	det4	36.67	202 ± 14	5.51 ± 0.39	1939.82 ± 136.49
sim2-12-DTL	det3	20.37	18 ± 4	0.88 ± 0.21	311.14 ± 73.34
	det4	20.37	78 ± 9	3.83 ± 4.34	1348.27 ± 152.66
sim2-13-DTL	det3	20.37	1676 ± 41	82.28 ± 2.01	285970.55 ± 707.65
	det4	21.20	8 ± 3	0.38 ± 0.13	132.85 ± 46.97

Table 11: Number of counts detected, c/bunch and c/μs for the fast nBLM modules for which we have the higher statistics in each scenario. The error is statistical error in the simulated number of events.

1% 1W/m in 14 Hz			Accidents
ESS input	nBLM	c/ms (kHz)	c/μs (MHz)
sim2-0	det3	0.008 ± 0.001	22.44 ± 2.54
sim2-1	det3	0.0024 ± 0.0005	10.65 ± 2.09
sim2-8	det1	1.04 ± 0.03	18569.94 ± 594.71
	det2	0.028 ± 0.006	495.20 ± 97.12
sim2-11	det3	0.015 ± 0.003	326.50 ± 56.00
	det4	0.091 ± 0.006	1939.82 ± 136.49
sim2-12	det3	0.015 ± 0.003	311.14 ± 73.34
	det4	0.063 ± 0.007	1348.27 ± 152.66
sim2-13	det3	1.48 ± 0.04	28970.55 ± 707.65
	det4	0.007 ± 0.002	132.85 ± 46.97

Table 12: Rates obtained for the nBLM fast modules simulated in each accidental scenario but normalizing to the case of 1% 1W/m, and distributed uniformly in 14Hz, as explained in the text.

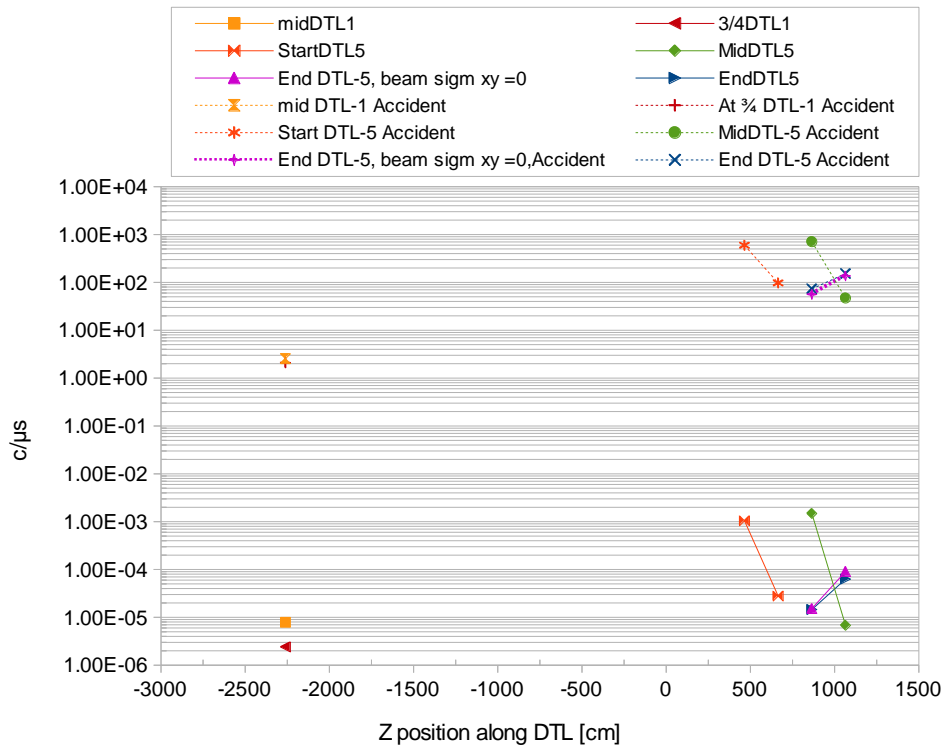




Figure 32: Comparison between the rates obtained in case of accidents (dashed lines) with respect normalizing them to 1W/m loss (solid lines), for the fast modules. They have been computed for different loss scenarios in which the nBLM fast detectors have been placed at different location around DTL-1 and DTL-5 (x-axis).

7.2. Conclusions for the 1W/m case and the accidental one rates

We have seen that the expected rates in case of a localized loss and the rates for a loss of 1% 1W/m are very different. Therefore, we can easily recognized an increment in the emitted neutrons in case of a problem within 1 μ s time response. In addition, with the fast module we are also capable to detect the increment in a much shorter time (few ns). We need to include here the time for the electronics and signal processing. From the FEE we expect an extra 100 ns. However, the huge rates expected based on the Montecarlo simulations, for some cases, are too high for individual event counting, as we are talking about GHz. There are several options to reduce these rates, which can be done during the commissioning phase:

- Reducing the B₄C thickness (range 150 nm – 2 μ m) \rightarrow factor more than 10 reduction
- Using natural Boron instead of ¹⁰B \rightarrow factor 5 reduction
- Detector segmented in 4, possibility to read from just 1 to the 4 strips \rightarrow factor 4

The combination of the three factors gives a reduction factor in the efficiency of 200. The first two options imply an intervention in the detector (dismounting, opening and closing the chamber, total time \sim 1 day). The third option needs access to the accelerator tunnel but no intervention to the

 	nBLM – PDR1.2	CEA-ESS-DIA-RP-0027
	ESS-I	Page 52 over 61

chamber. Depending on the final design, it could be a change of a jumper position, or replacement of a plug-n-play card or a simple change of the cable connection.

An alternative way to change the sensitivity during operation and without accessing the accelerator tunnel is to change from counting to current mode. This can be done by simply changing the applied high voltages, but it requires a modified version of the software and firmware. The effect on the sensitivity of the system will be estimated only after performing the planned tests or even during the commissioning phase (if this option is included in the final system).

During a loss of 1% of 1 W/m the lowest expected rate is of few kHz for the slow detector. In case we reduce the efficiency, this rate will be of few Hz. In the case of the fast detector, as the efficiency is lower, we have obtained in the standard geometry rates of few c/s.

These results imply several things. First of all, the operational settings (the gain of the detector) will be different at different accelerator locations. In addition, there are several methods to tune the efficiency, as explained, during commissioning. The tests at LINAC4 will also help for this. Moreover, we may need to define some detectors for monitoring (higher gain, will saturate during an accident) and others with the settings for the detection of a loss (lower gain, probably insensitive during normal operation, can handle the higher rates expected in case of an accidental loss).

7.3. Threshold between “thermal” and fast neutrons

In [5] it is suggested two possible thresholds to separate between “thermal” and fast neutrons. They corresponds to 0.5 MeV or 50 keV. This is naturally obtained in the fast detector as we can see in Figure 33. The detector is only sensitive to initial neutrons energies of $\sim > 0.2$ MeV. In the case of the slow we have some margin playing with the Mirrobor thickness (section 7.4), however, the limits suggested in [5] seems quite unrealistic as will imply a high efficiency loss.

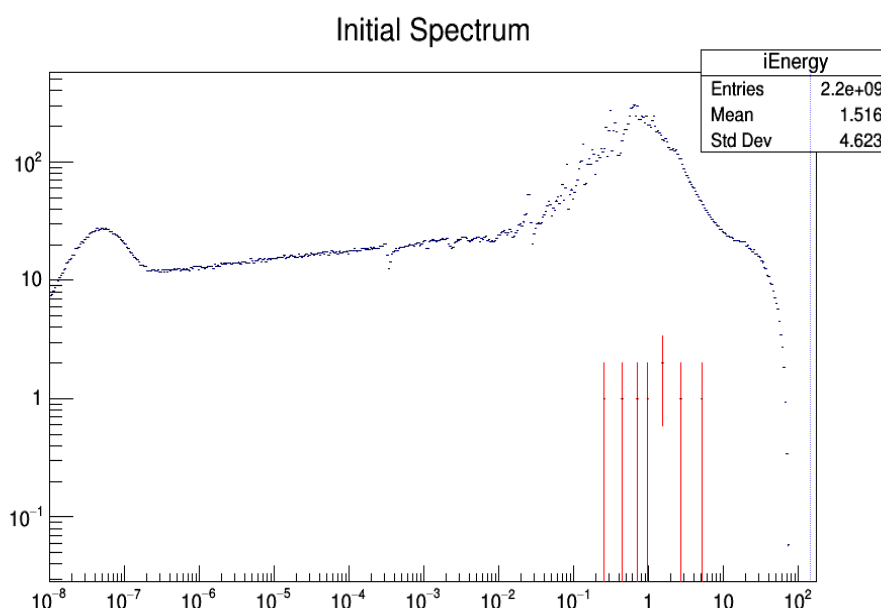


Figure 33: Initial spectrum (in blue) compared with the neutrons that deposited energy in the nBLM fast detector (red). The detector was placed on top of the DTL-5 when using the scenario sim2_13 corresponding to a lost in the middle of DTL-5. The x-axis represents the initial neutron energy in MeV. As we can see we are only sensitive to initial neutrons energies of ~ 0.2 MeV.

7.4. Detector position results by simulations

Several positions have been studied following the recommendations in [5] regarding the DTL accelerator sections. In previous section, all results were obtained placing the detectors on top of the accelerator with the detector facing the top of the beam, as sketched in Figure 34. In this figure we show the slow module with a double face detector in the middle of the chamber, i.e. with two conversion regions. The fast detector has been also simulated with the drift region facing towards the accelerator.

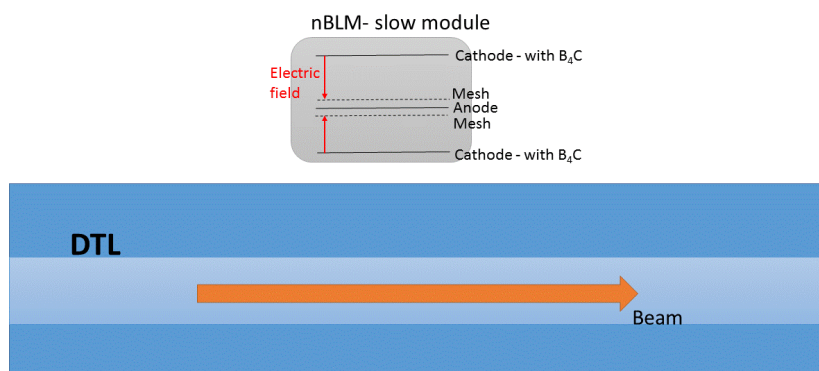




Figure 34: Sketch of the position of the nBLM slow module in the simulations studying the response to the ESS scenarios. This corresponds to the position on top of the accelerator. Other simulations have been carried out placing them on the lateral, with the drift or conversion region facing the beam or in the space between the DTL tanks (in this case only the fast response was studied due to space restrictions in this area).

The slow and fast module have been placed at 0, $\frac{1}{4}$, $\frac{2}{4}$, and $\frac{3}{4}$ of the total length of the tank under study, either DTL-1 or DTL-5. That means within a separation of 2m one from the next. The rates detected at the position of the loss were always higher than in the neighbour detectors. This difference is more or less proportional to the distance between them.

Some of the scenarios were also simulated placing the detectors on the lateral or on the space between the DTL tanks (*in-between* detectors). Results are largely discussed in [1]. Here we summarized the main conclusions:

- For **the lateral detectors** we simulated scenarios sim2_0 (lost at middle of DTL-1) and sim2_13 (loss at middle DTL-5).
 - Both the fast and slow detector response were studied and compared with the top location.
 - For the slow detectors, the rate is slightly higher if they are located on the top, of about a factor 2 in the position of the lost for DTL-1 but pretty much the same in all locations for DTL-5 (just a factor of 1.3 maximum).
 - While for the fast modules it is also slightly higher for the top detectors, of about a factor 2-5 in the position of the lost but just a difference of 0.5 away from the lost location, however we have not too much statistic to compare more than 2 points and it is difficult to conclude anything.

 	nBLM – PDR1.2	CEA-ESS-DIA-RP-0027
	ESS-I	Page 55 over 61

- For **the in-between detectors**, four lost scenarios have been used as input: an accident in the middle of DTL-1 (sim2_0), and accident at $\frac{3}{4}$ of DTL-1 (sim2-1), and an accident at the end of DTL-5 (sim2-11 and sim2-12).
 - In this case we only simulated the fast module because we are especially interested in the fast response of the system at these locations, and the slow one dimensions are too big to be placed there.
 - Even simulating about 2×10^9 initial neutrons, only the losses happening very close to the detectors could be registered. In general, we also see some counts in the next tank one, but with very little statistics (only 1-2 events).
 - For example, for a lost in the middle of DTL-1 the detector placed between DTL-1 and DTL-2 already detect few events/ μ s, being its detection increased by a factor 90 when the lost happen at 2m from the end of DTL-1 (~ 90 MHz).
 - Similarly, when the lost occurred at the end of DTL-5 the detector placed at the end of it, detects a rate of about 5GHz, while the one placed between tanks 4 and 5 has a very low statistics.
 - In general we can say that the detectors placed in-between the tanks where the lost happen and in between the next ones will be the ones being able to detect the lost and the sensitivity will be different depending where along the tank the lost has happened.

For the normal operation, there are “hot spots” where will be more interesting to locate the detector due to a high probability of losses.

In conclusion, as agreed in the kick-off meeting, ESS will decide about the positions of the detectors. The aim of this section is to show, that, from simulations studies, the response if placing the detectors on top or on the lateral of the accelerator do not change much. In addition, information about the location of the loss seems to be accessible when analysing the rate of more than one detector, i.e., considering all the modules as a system. Moreover, the placing of the detectors in the region between the DTLs give us also high detectable rates in case of accidents. The study of the response of the nBLMs in other accelerator regions than the DTLs have not been possible to be done as the input scenarios from ESS corresponded only to the DTL1 and 5 region.

7.5. Using borated rubber instead of Cd

A study using borated rubber instead of Cd was done. We can summarize the expected efficiency in Figure 35 for 1mm Cd compared with different thickness of MirroBor when simulating an isoethargic distribution of neutrons with a 2π initial angle distribution. In Figure 35 right we can see the time resolution of the detector and how it does not change compared with the use of Cd.

When using sim2_13 as input file for det3 results are shown in Figure 36. Even if the increase of the Mirrobor thicknesses decreases the thermal neutron efficiency, we are far to be over the suggested threshold of 50 keV if we want to keep a reasonable efficiency.

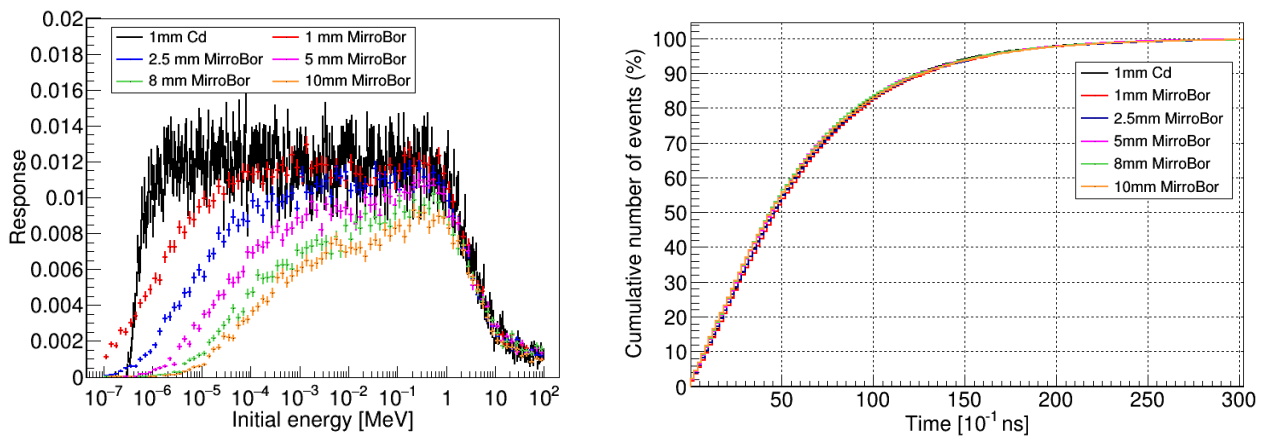


Figure 35: (left) Response to an initial flux of neutrons isoethargic distributed between 0.1eV to 100 MeV. The response is shown for different thicknesses of mirrobor (1mm in red, 2.25 mm in blue, 5mm in magenta, 8 mm in green and 10 mm in orange) compared with the case of 1 mm Cadmium (black). (Right) Comparison of the time response between the same cases.

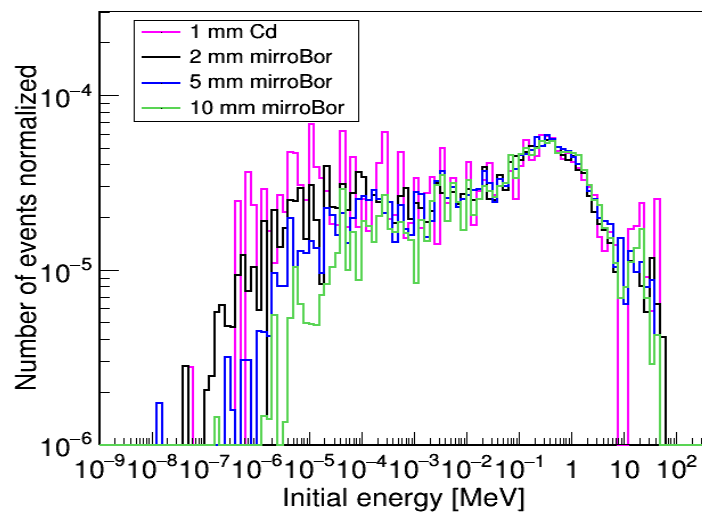





Figure 36: The response of the slow module placed on top of the lost (middle of DTL-5) is shown for different mirrobor thicknesses.

 	nBLM – PDR1.2	CEA-ESS-DIA-RP-0027
	ESS-I	Page 57 over 61

8. Recompile of points to discuss

In this section we list the different points or aspects to focus the discussion. Here we just summarized them, for more details go to the referenced section of this document.

1. Prototypes: Section 2.4, signal pulse duration and rise time (100/30 ns).
2. Prototypes: Section 2, O-ring used in prototype approved for CERN, ok also at ESS?
3. Electronics: Section 3.1: Chose between plug-n-play card or all elements on board
4. Electronics: Section 3.1: 1-4 readouts independents or sum.
5. Electronics: Section 3.1, decision on cables, one or more signal outputs per detector?
6. Gas system: Section 4.1, final connection to detector by polyethylene tubes?
7. Gas system: Section 4.2.1, use of premixed bottles
8. Gas system: Section 4.2.2, decision taken about the place of the installation of gas system
9. Gas system: Section 4.2.3, use fast closing valve or extra tube with hand valve for detector connections
10. Gas system: Section 4.3, not received yet list of components from ESS
11. Gas system: Section 4.3, can we use Profibus for the PLC?
12. Controls-Acquisition: Section 5, How we do communication with MPS? Which output from FPGA? Rates or binary alarm output?
13. Controls-Acquisition: Section 5, Does it exist analogical output cards to communicate?
14. Speed communication between CPU cards.
15. Controls-Acquisition: Section 5, Do coincidence algorithms into FPGA that controls neighbour detectors?
16. Integration: Section 6.1, whole modules or individual detectors with different objective?
17. Integration: Section 6.1, extra power supply for SY crate? (redundancy/cost)
18. Integration: Section 6.1, define control system for 35 modules or 42? Implies different number of ADC cards, etc.
19. Integration: Section 6.1, **need to decide about location of detectors**
 - a. Impact on electronics, gas system, power supplies, ...
 - b. More than 2 modules per DTL?
20. Response to ESS scenarios: Section 7.2, implement version in software for current mode?
21. Response to ESS scenarios: Section 7.2, use of fast modules or not? (necessity in order to observe beam structures)
22. Response to ESS scenarios: Section 7.1, more studies for normal scenarios needed?
23. General: **System specifications and additional costs**

	nBLM – PDR1.2	CEA-ESS-DIA-RP-0027
	ESS-I	Page 58 over 61



9. Answers to questions from PDR1.1 review

To the comments:



- Is it possible to build up statistics with fast detector such that over many pulses, to have loss vs time with very good time resolution?
 - Detector has the response to do it (ns).
 - However, uncertainty due to the difference in the flight path depending on the source of the loss. If coverage dense, then better resolution.
 - Probably 100 ns resolution can be realistic.
- What is the time resolution of the slow detector? This is important for optimizing linac tune with pulses in diagnostics mode.
 - 100% of events detected in 100 μ s.
 - Maybe enough signal in 1 μ s (4cm polyethylene).
 - However a lot of delayed signal not allow to see structures within the pulse
- Consider if the fast module can be eliminated?
 - To be decided with ESS depending on decision about studying small structures of loss. See answer before.
- It was not clear how to estimate the RF-induced photon background?
 - Yes, this is why we plan to:
 - Test with cryogenics modules at CEA
 - Test at LINAC4
 - Test with RF cavities at ESS during its commissioning? Depends on the availability of nBLM electronics
- Does CEA have enough information on the radiation environment to the electronics?
 - No

To the answers:

- ESS Lund team should send list of standard gas handling systems to Saclay Controls.
 - Not received yet
 - However we had a VC in May 2017, approved use of Swagelok. ESS working on list of components, waiting document.
 - CEA has sent a list of possible cards, waiting approval
- Saclay team should provide the Lund team the expected pulse shapes for software development
 - Sent pulses for neutrons and for sparks in November 2016
 - Sent Requirements document describing signal and possible analysis in May-2017. No feedback received yet.

 	nBLM – PDR1.2	CEA-ESS-DIA-RP-0027
	ESS-I	Page 59 over 61

- Saclay team should provide the Lund team the expected resolution and voltage level for digitizer selection
 - Decision on digitizers in April, use of ADC_3111
- There should be a follow up on the Linkoping contact.
 - ToDo
- Take advantage of cryomodule tests at Saclay to test detector. Consider including ion chambers in this test along with nBLMs
 - Foreseen after summer
- Consider a test at SNS, maybe supported by Sasha Zhukov?
 - Not foreseen in the project's budget

 	nBLM – PDR1.2	CEA-ESS-DIA-RP-0027
	ESS-I	Page 60 over 61

10. Bibliographie

- [1] L. Segui, "MonteCarlo results: nBLM response to ESS scenarios," ESS-0107320 / CEA-ESSDIA-RP-0023, 2017.
- [2] I. Giomataris and al, "Micromegas in a bulk," *Nuclear Instruments and Methods in Physics Research Section A: Accelerators, Spectrometers, Detectors and Associated Equipment*, vol. 560, no. 2, pp. 405-408, 2006.
- [3] L. Segui and et al., "Requirements and function for the nBLM control system," CEA-ESS-DIA-RP-0024, 2017.
- [4] S. Aune, L. Segui and T. Papaevangelou, "Gas Pipes nBLM system," CEA-ESS-DIA-NT-0020, 2017.
- [5] I. Dolenc Kittelman, "Report regarding the MC simulation for BLM-focus on the nBLM," CHESS, ESS-0066428, 2016.
- [6] L. Segui, "Cable specifications for nBLM system," CEA-ESS-DIA-NT-0021, 2017.
- [7] L. Segui, "nBLM PDR1.1," CHESS, ESS-0087794, CEA-ESS-DIA-RP-0013, 2016.
- [8] "MiroTron," [Online]. Available: <http://www.mirrotron.kfkipark.hu/shield.html>.
- [9] Y. I. Levinsen, "ESS 2015 Baseline Latitice Error Study," CHESS ref. ESS-0049433, 2016.

Appendix 1

List of simulations from the BI group used as input in our studies.

sim Name	#primaries	uniform loss		normal operation		localized loss							mesh files	production cuts	edep refined	comment
		beam theta [mrad]	tunnel in	tunnel in	MEBT loss included	gun theta [mrad]	Beam sigmXY [mm]	gun phi [deg]	gun energy [MeV]	geo element	el. Fraction	comment				
sim0-0	100 M +1	1	yes										11	e,gamma: 10um p: 0	no (default)	
sim0-1	100 M +1	1	no										11	e,gamma: 10um p: 0	no (default)	
sim1-0	800 M +1			yes	yes								11	e,gamma: 10um p: 0	no (default)	
sim1-1	800 M +1			yes	no								11	e,gamma: 10um p: 0	no (default)	
sim1-2	800 M +1			no	no									e,gamma: 10um p: 0	no (default)	
sim2-0	600 M +1					50 (max in DTL1)	1	0	11.5	106	0.5	mid DTL1	0	e,gamma: 10um p: 0	yes	
sim2-1	100 M +1					50	1	0	17.9	140	0.5	at 3/4 DTL1	0	e,gamma: 10um p: 0	yes	
sim2-2	1000 M +1					50	1	0	7.6	78	0.5	at 1/4 DTL1	0	e,gamma: 10um p: 0	yes	
sim2-3	600 M +1					50	1	-90	11.5	106	0.5	mid DTL1	0	e,gamma: 10um p: 0	yes	
sim2-4	700 M +1					2	1	0	7.6	78	0.5	at 1/4 DTL1	0	e,gamma: 10um p: 0	yes	too little hits
sim2-5	1300 M +1					50	0	0	7.6	78	0.5	at 1/4 DTL1	3	e,gamma: 10um p: 0	yes	
sim2-6	1300 M +1					10	0	0	5.8	78	0.5	at 1/4 DTL1	2	e,gamma: 10um p: 0	yes	
sim2-7	1300 M +1					10	1	0	5.8	78	0.5	at 1/4 DTL1	2	e,gamma: 10um p: 0	yes	
sim2-8	40M +1					10 (max in DTL5)	0	0	71.8	342	0.5	start of DTL5	2	e,gamma: 10um p: 0	yes	
sim2-9	40M +1					10	1	0	71.8	342	0.5	start of DTL5	2	e,gamma: 10um p: 0	yes	
sim2-10	40M +1					5	0	0	69.8	342	0.5	start of DTL5	2	e,gamma: 10um p: 0	yes	
sim2-11	40M +1					10	0	0	86.5	384	0.5	end of DTL5	2	e,gamma: 10um p: 0	yes	
sim2-12	40M +1					10	1	0	86.5	384	0.5	end of DTL5	2	e,gamma: 10um p: 0	yes	
sim2-13	40M +1					10	0	0	79.3	364	0.5	mid DTL5	2	e,gamma: 10um p: 0	yes	